A Dissertation for the Degree of Doctor of Korean Medicine

Anti-obesity Effects of Lignan-enriched Nutmeg Extract in High-fat Diet Mouse

Major in Korean Internal Medicine III

Department of Korean Medicine

Graduate School, Daejeon University

by

Jae Ho Yang

February 2024

	Anti-obesity Effects of Lignan-enriched Nutmeg Extract in High-fat Diet Mouse			**Jae Ho Yang**		**2024**	

Anti-obesity Effects of Lignan-enriched Nutmeg Extract in High-fat Diet Mouse

A Dissertation Submitted to the Graduate School
in Partial Fulfillment of Requirements
for the Degree of Doctor of Korean Medicine

December 2023

Thesis Supervisor Hwa-Seung Yoo

Department of Korean Medicine, Graduate School, Daejeon University

by

Jae Ho Yang

This certifies that the dissertation

of Jae Ho Yang is approved.

Anti-obesity Effects of Lignan-enriched Nutmeg Extract in High-fat Diet Mouse

December 2023

Committee Chair	Joo Jong-cheon
Committee Member	Park Soo-jung
Committee Member	Lee Yeon-weol
Committee Member	Park Ji-hye
Committee Member	Yoo Hwa-seung

Graduate School, Daejeon University

Contents

List of Tables

List of Figures

Abbreviations

AMPK	AMP-activated protein Kinase
BCA	BicinChoninic Acid
BMC	Bone Mineral Content
BMD	Bone Mineral Density
C/EBP-α	CCAAT-Enhancer-Binding Proteins-alpha
CID	Collision-Induced Dissociation
Cyp7a1	Cholesterol 7α-hydroxylase
DEGs	Differentially Expressed Genes
DEPs	Differentially Expressed Proteins
DEXA	Dual Energy X-ray Absorptiometry
DTT	DiThioThreitol
ESI	ElectroSpray Ionization
ExDEGA	Excel-based Differentially Expressed Gene Analysis
FDR	False Discovery Rate
FE	Fold Enrichment
GLP-1	Glucagon-Like Peptide-1
GO	Gene Ontology
GOBP	Gene Ontology Biological Process
HDL	High Density Lipoprotein
HFD	High-Fat Diet
H&E	Hematoxylin and Eosin
IAA	IodoAcetAmide
IL	InterLeukin
KEGG	Kyoto Encyclopedia of Genes and Genomes
LDL	Low Density Lipoprotein
LNX	Lignan-enriched Nutmeg eXtract

LNX-HFD	LNX-fed High-Fat Diet
MS	Mass Spectrometry
MSe	enhanced Mass Spectrometry
NAFLD	Non-Alcoholic Fatty Liver Disease
NASH	Non-Alcoholic Steato-Hepatitis
ND	Normal Diet
PDB	Protein Data Bank
PPAR	Peroxisome Proliferator-Activated Receptor
SDS-PAGE	Sodium Dodecyl Sulfate-PolyAcrylamide Gel Electrophoresis
SREBP	Sterol Regulatory Element-Binding Protein
STAT3	Signal Transducer and Activator of Transcription 3
TCHO	Total Cholesterol
TFA	Tri-Fluoro-Acetic acid
TG	Total Glycerides
TNF-α	Tumor Necrosis Factor-alpha
UPLC	Ultra Pressure Liquid Chromatography

I. Introduction

Obesity is a distinctive phenotype where an excessive accumulation of body fat has temporarily adverse effects on health (Powell-Wiley et al., 2021). Excessive fat accumulation triggers non-alcoholic fatty liver disease (NAFLD), inducing neutral fat buildup in the liver, leading to inflammation, liver fibrosis, and in severe cases, progression to liver cancer (Cohen et al., 2011). Obesity, characterized by excessive fat accumulation, is associated with various diseases beyond liver conditions. For instance, cardiovascular diseases, type 2 diabetes, dyslipidemia, and various cancers originate from obesity (Haslam and James, 2005). In particular, type 2 diabetes manifests due to insulin resistance, involving pathological toxicity in fatty liver, accompanied by lipid breakdown in adipose tissue and *de novo* fat synthesis in liver (Saponaro et al., 2015). Obesity is recognized as a preventable cause of premature death on a global scale, with approximately 600 million adults (12%) and 100 million children reported as obese in 195 countries according to 2015 statistics (Afshin et al., 2015). Today, most Western European countries, the United States, Japan, and others, excluding the United Kingdom, consider obesity as a disease and actively manage it through governmental interventions (Jensen et al., 2014).

Obesity arises from individual, socioeconomic, and environmental factors, with an improper diet being a common cause. Obesity occurs when there is an imbalance between energy intake and expenditure in metabolic processes (Ghanemi et al., 2018). Improving the quality of the diet can help manage obesity to some extent. For example, reducing the intake of high-calorie foods rich in fats or sugars and increasing the relative consumption of dietary fiber can contribute to obesity reduction. Prescription of anti-obesity drugs along with appropriate diet can prevent obesity, as pharmacological actions reduce appetite or inhibit fat absorption (Yanovski and Yanovski, 2014). In cases where achieving results through diet, exercise, or medication is challenging, alternative methods such as intra-gastric balloon insertion, gastric bypass surgery, or surgeries that involve partial removal of the stomach can reduce food intake and induce early satiety, but they come with associated risks (Colquitt et al., 2014). Although the development of anti-obesity drugs has been predominantly led by global pharmaceutical companies, concerns persist regarding additional side effects beyond partial efficacy that need to be addressed (Müller et al., 2022).

The most notable characteristic of obesity is the resetting of the positive energy balance to a new high level, making it challenging to treat (Schwartz et al., 2017). The biological mechanisms underlying this process remain ambiguous, and ongoing research aims to elucidate them. Several known biological mechanisms contribute to the development and maintenance of obesity. One remarkable aspect involves the discovery of leptin and ghrelin, two hormones that regulate appetite through the central nervous system. Leptin, produced in adipocytes, regulates long-term energy balance (Al-Hussaniy et al., 2021). Leptin levels influence appetite and satiety, sending signals towards energy storage, primarily breaking down neutral fat stored in adipose tissue. Leptin levels, when decoded in the brain during a state of starvation, trigger metabolic, endocrine, neurochemical, and behavioral changes (Hebebrand et al., 2022). Ghrelin, known as the hunger hormone, is produced in the gastric tissues, particularly in the endocrine cells of the stomach, and stimulates appetite (Kojima et al., 1999). Ghrelin performs preparatory processes for food intake, enhancing gastrointestinal motility, stimulating gastric acid secretion, and activating neuropeptide Y neurons that initiate appetite (Müller et al., 2015).

Leptin gene (*ob*) mutations gradually manifest the traits of obesity, making *ob/ob* mice a research model for obesity (Zhang et al., 1994). Leptin secreted from adipose tissue communicates appetite-related signals to the hypothalamus, regulating feeding behavior (Jequier, 2002). *Ob/ob* mice, a model organism, exhibits traits of obesity, insulin resistance, and gradual development of liver fibrosis after four weeks of age. Therefore, *ob/ob* mice are utilized not only for obesity studies but also for research on related conditions such as diabetes and liver dysfunction (Trak-Smayra et al., 2011). However, the *ob/ob* mouse model takes considerable time for the observation of obesity traits due to leptin gene mutations, while high-fat diet-induced obesity in mice results in relatively rapid changes in energy metabolism (Fiedman and Halaas, 1998; Wong et al., 2016). Using high-fat diet mouse models for obesity research offers the advantages of experimental control, rapid induction of metabolic disorders, tracking of hepatic metabolic processes, and efficient screening for obesity-centric drugs (Anstee and Goldin, 2006). Therefore, this study aims to induce obesity in mice through a high-fat diet and investigate the anti-obesity effects of nutmeg extract. Nutmegs have a history of reports regarding their toxic effects (Cushny, 1908).

Nutmeg seed of the *Myristica* genus evergreen tree, has a documented history of use in the Indonesian archipelago dating back to 3500 years ago (Lape et al., 2018). The spice spread to India in the 6th century and was introduced to European trade through Arab merchants in the 13th century. Nutmeg has been traditionally used as a herbal remedy to alleviate symptoms such as indigestion, abdominal pain, vomiting, and loss of appetite, but excessive consumption can lead to psychoactive effects (Ehrenpreis et al., 2014). The seeds of the nutmeg contain toxic substances, myristicin and elemicin, inducing hallucinations (McKenna et al., 2004). However, recent research has developed methods to reduce the major toxic substance, myristicin, and concentrate the effective compound, lignan (Lee et al., 2023). In brief, lignan-enriched nutmeg extract (abbreviated as LNX) was prepared by two-step ethanol extraction as previously conducted (Nguyen et al., 2010). Various effective lignan compounds such as nectandrin B (majority), verrucosin, fragransin A2 were 6.1% dry weight and, conversely, myristicin as a typical toxic compound was observed less than 0.04%. By *in vivo* mouse model and *in vitro* cell experiments, LNX has been reported to have muscle-improving effects and anti-obesity effects, respectively (Lee et al., 2023; Perumal et al., 2023). In particular, among the lignan components, nectandrin B activates AMPK, inhibiting aging and extending the lifespan of fruit flies (Jang et al., 2019; Ahn et al., 2023). Notably, nutmeg-derived nectandrin B has been reported to have anti-obesity effects at the cellular level by activating AMP kinase (Nguyen et al., 2010; Hien et al., 2011). However, preclinical or clinical-level studies on the anti-obesity effects of nectandrin B or LNX have not been conducted yet.

This study divided 9-month-old C57BL/6 male mice into groups with normal diet (ND), high-fat diet (HFD), and high-fat diet supplemented with 0.01% or 0.1% LNX (LNX-HFD), and observed physiological and serum characteristics every three months. In addition, the study analyzed the expression patterns of total mRNA and proteomes in liver tissues to observe changes related to lipid metabolism. Typically, liver tissue is significantly influenced by prolonged high-fat diet consumption, leading to substantial effects on lipid and cholesterol metabolism. Additionally, since the major metabolic processes of external substances (biotransformation and detoxification) occur in the liver, physiological changes can be tracked and observed through omics analysis (Kirpich et al., 2011). While there have been previously transcriptomic studies to understand the toxic mechanisms of Non-Alcoholic Steato-Hepatitis (NASH), data interpretation has been limited due to discrepancies between actual protein expression and transcriptomes (Aegidius et al., 2020; Wang et al., 2019). Quantitative proteomic

analysis adds to the discovery of the biomarkers for fatty liver and studying correlations with transcriptomes, providing insights into the systematic exploration of the anti-obesity effects of LNX, especially in the context of naturally induced obesity through a high-fat diet. The goal of this research is to systematically elucidate the anti-obesity effects of LNX through comparative profiling of transcriptomes and proteomes, exploring new mechanistic interpretations, and investigating the potential for anti-obesity treatment at the molecular level.

II. Materials & Methods

1. Experimental animals

All experimental procedures involving animals were approved by the Animal Ethics Committee of the KBSI Gwangju Center (Approval Number: KBSI-IACUC-23-12). Nine-month-old male C57BL/6 mice were used in the study, and they were provided free access to water and standard chow. The animal housing conditions were maintained at a temperature of 22~24°C, humidity at 55±5%, and a 12-hour light/dark cycle. The control group (ND) was fed a diet containing 4% fat, 30% protein, and 58% carbohydrates (LabDiet 5L79, Orient Bio, Inc., Seongnam, Korea), with a total caloric content of 3.88 kcal/g. The experimental group (HFD) received a high-fat diet containing 24% fat, 24% protein, and 46% carbohydrates (D12451, Research Diets, New Brunswick, NJ), with a total caloric content of 4.96 kcal/g (**Table 1**).

A schematic diagram of the experimental design is presented in **Figure 1**. The animals were categorized into the control group (ND, n=4), experimental group (HFD, n=10), and high-fat-Diet supplemented with 0.01% or 0.1% LNX (HFD-LNX-Low, HFD-LNX-High, each n=10). The mice were allowed free access to food and water. Body weight, food intake, and water consumption were measured at the beginning of the experiment and at 3-month intervals. Blood analysis and real-time quantitative analysis of body composition (fat, bone) were conducted. At the end of 6 months, mice were anesthetized by isoflurane inhalation, and visceral adipose tissue and the left lobe of the liver were extracted for subsequent experiments. Tissues were stored at -80°C for RNA-Sequencing and proteomic experiments.

Table 1. Composition of high-fat diet for feeding mouse

Ingredient	ND	HFD*	LNX (0.01%)-HFD	LNX (0.1%)-HFD
Casein, 80 Mesh	200	200	200	200
L-Cystine	3	3	3	3
Corn Starch	72.8	72.8	72.8	72.8
Maltodextrin 10	100	100	100	100
Sucrose	172.8	172.8	172.8	172.8
Cellulose, BW200	50	50	50	50
Soybean	25	25	25	25
Lard	0	177.5	177.5	177.5
Mineral Mix	10	10	10	10
Dicalcium Phosphate	13	13	13	13
Calcium Carbonate	5.5	5.5	5.5	5.5
Potassium Citrate	16.5	16.5	16.5	16.5
Vitamin Mix	10	10	10	10
Choline Bitartrate	2	2	2	2
FD&C Red Dye #40	0.05	0.05	0.05	0.05
LNX	0	0	0.086	0.86
Total (g)	680.65	858.15	858.15	858.15
Calorie (kcal/g)	3.88	4.96	4.96	4.96

*Rodent Diet with 45 kcal% Fat HFD (Catalog # D12451)

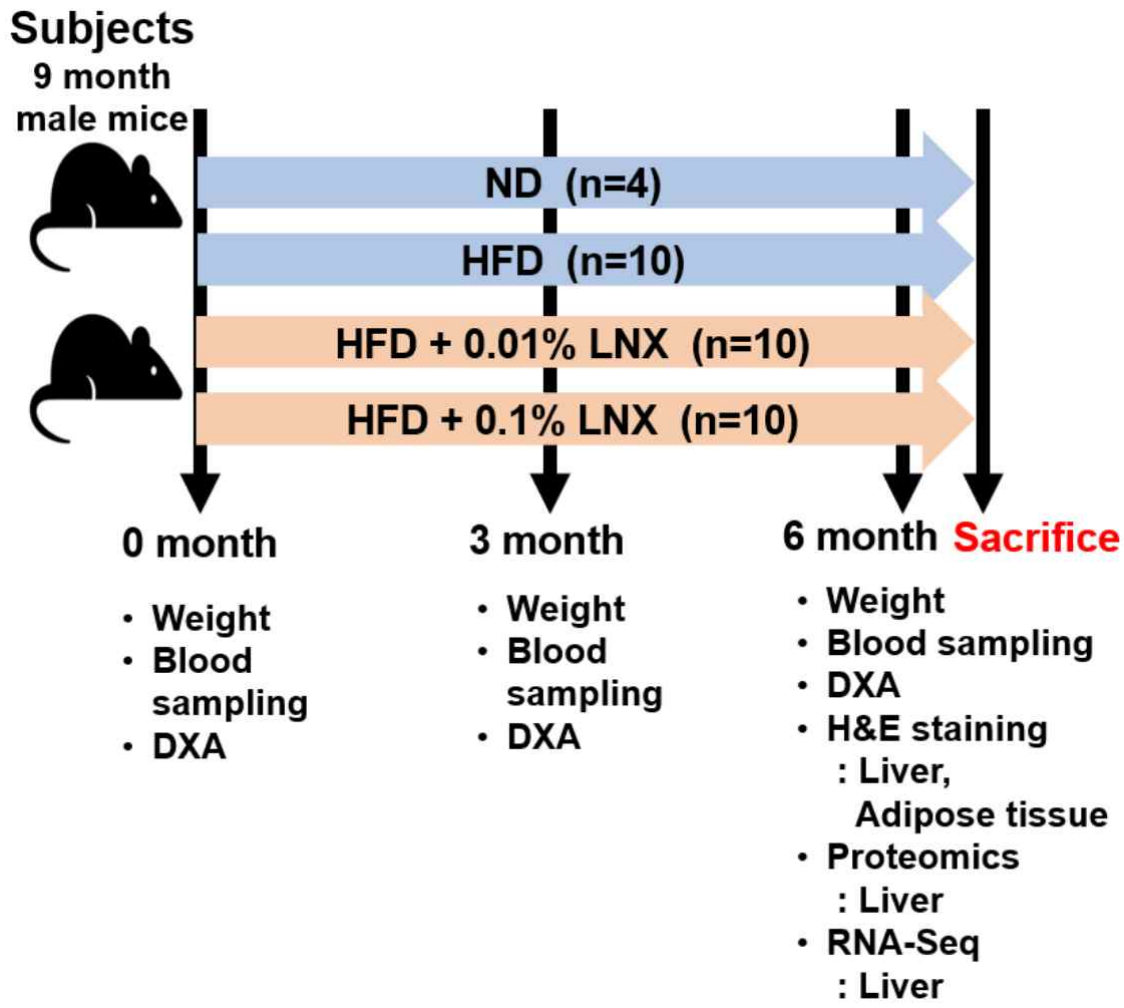

Figure 1. Scheme of experimental design for this study. At every 3 month (0, 3, 6 month), body weight, blood biochemistry and body components were measured. At final 6 month, experimental mice were sacrificed to extract liver (left lateral lobe) and visceral fat tissue for transcriptomic and proteomic analyses.

2. Analysis of Lignan Compounds in LNX

The powder of 1 mg LNX sample was dissolved in 1 mL of distilled water and diluted at a ratio of 1:100. The diluted solution was vortexed for 30 min, filtered through a 0.22 μm syringe filter, and analyzed using Q-Exactive Plus mass spectrometer (Thermo Fischer Scientific, Waltham, MA, USA). The analysis utilized a column (Acquity UPLC peptide CSH C_{18}, 130Å, 1.7 μm, 2.1 X 100 mm) under conditions of 25°C. Solvent A consisted of 0.1% formic acid, and solvent B was acetonitrile. Solvent B was delivered at a flow rate of 0.35 mL/min with a 40% composition, and 5 μl of the analyte was injected. The analytes were ionized by electrospray ionization (ESI) and fragmented using collision-induced dissociation (CID). Mass analysis was performed using a TOF analyzer under positive ion-mode conditions with a cone voltage of 40 V. Mass scans were conducted in the 100-2000 *m/z* range using the MSe mode. Peaks corresponding to the standard substance nectandrin B were identified from the UV chromatogram and MS chromatogram, and the structural information of nectandrin B was interpreted through MS/MS analysis.

3. Histological Analysis

Liver and visceral adipose tissues were fixed overnight in 10% neutral buffered formaldehyde (Sigma-Aldrich, MA, USA). Tissues were dehydrated through a series of ethanol solutions with increasing concentrations and embedded in paraffin. Sections of 5 μm thickness were cut after paraffin removal, stained with hematoxylin-eosin (H&E, Sigma-Aldrich, MA, USA), and sealed with mounting media (Vector Laboratories, CA, USA). Images were captured using a visible and fluorescent slide scanner (KF-FL-005, KFBio, ZheJiang, China). Quantitative analysis of fat content was performed using the digital image analysis software Image J, representing positively stained areas as a relative percentage of the entire tissue section. Histological quantification data were analyzed using GraphPad Prism software (GraphPad, La Jolla, CA, USA). All statistical analyses were reported as mean ± SEM. Mann-Whitney statistical analysis was performed using R software, and statistical significance was determined at levels of $P<0.05$, $P<0.01$, or $P<0.001$.

4. Biochemical and Body Composition Analysis

Blood glucose levels were measured using blood glucose test strips and a portable blood glucose meter (Accu-Chek Active, Roche Diagnostic GmbH, Mannheim, Germany). Blood concentrations of triglycerides (TG), total cholesterol (TCHO), high-density lipoprotein cholesterol (HDL-CHO) were measured using commercial kits (Asan Pharmaceutical, Seoul, Korea). Low-density lipoprotein cholesterol (LDL-CHO) levels were calculated using the Friedewald formula '[(LDL-CHO) = (TCHO) - ((HDL-CHO) - (TG)/5)]' (Hong et al., 2023).

For body composition analysis, experimental animals were weighed after receiving inhalation anesthesia with isoflurane. Dual-Energy X-ray Absorptiometry (DEXA, Medikors, Seongnam, Korea) was used to scan the entire body. Scan data were used to capture the internal structure of the whole body and generate pseudo-colors for bone (white) and fat areas (red). Measurements such as fat weight, lean body mass, body fat%, bone area, bone volume, and bone mineral content (BMC) were quantitatively measured using dedicated software (InAlyzer, Medikors, Seongnam, Korea). All statistical analysis values were reported as mean ± standard deviation. Statistical analysis was performed using the Mann-Whitney test with R software, and statistical significance was determined at levels of $P<0.05$, $P<0.01$, or $P<0.001$.

5. RNA Sequencing

Liver tissue (15 mg of the left lobe) was homogenized, and RNA was extracted using TRIzol reagent (Invitrogen, MA, USA). The quality of RNA was assessed using the Agilent TapeStation system (Agilent Technologies, Amstelveen, Netherlands), and RNA quantification was performed using Qubit (Thermo Fischer Scientific Inc., DE). For the experimental animal groups' RNA, QuantSeq 3’-mRNA-Seq library construction was carried out using the QuantSeq 3’-mRNA-Seq Library Prep Kit (Lexogen, Inc., Austria) according to the manufacturer's protocol. Briefly, total RNA from each experimental animal was fragmented, and reverse transcription was performed using oligo-dT primers incorporating Illumina-compatible sequences at the 5'-end. After breaking down the RNA template, a random primer incorporating

the Illumina-compatible linker sequence at the 5'-end was ligated, resulting in the generation of a double-stranded library. The double-stranded library was purified using magnetic beads to remove all reaction components. The library was then amplified to add the complete adapter sequence required for cluster generation. The final library was purified from PCR components. The completed library underwent high-speed sequencing through single-end 75 base pair sequencing on the NextSeq 550 (Illumina Inc, San Diego, CA, USA).

QuantSeq 3'-mRNA-Seq sequence reads were aligned using STAR (Dobin et al., 2013). The STAR index was generated from representative transcript sequences for aligning to the genome assembly or for aligning to the transcriptome and was used for alignment files. These alignment files were used to assemble the transcriptome, estimate their abundance, and detect differential expression of genes. Differential gene expression based on counts from unique and multiple alignments was determined using HTSeq-count (Anders et al., 2015) with coverage. The read count (RC) data were processed within R using the Bioconductor package Edge R with TMM+CPM normalization (Gentleman et al., 2004). Gene classification was performed using software for searching DAVID (http://david.abcc.ncifcrf.gov/) and the Medline database (http://www.ncbi.nlm.nih.gov). Data mining and graphical visualization were performed using ExDEGA (Ebiogen, Seoul, Korea).

6. Protein Sample Preparation

Mouse liver tissue was prepared using a slightly modified version of the previous mouse skeletal muscle sample preparation method (Lee et al., 2023). In brief, approximately 50 mg of liver tissue was homogenized in 500 μL of mammalian protein extraction buffer (GE Healthcare, Chicago, IL, USA) and centrifuged at 16,000 g for 10 minutes. The supernatant was collected, and protein quantification was performed using the BCA assay kit (Thermo Fischer, Seoul, Korea). Each protein (10 μg) was electrophoresed in a 12% SDS-PAGE gel and stained with Coomassie Brilliant Blue G250. The entire gel was quartered, and proteins within the gel were cut into peptides using the in-gel trypsin digestion method (Shevchenko et al., 2006). In-gel proteins were reduced with DTT and alkylated with IAA. Trypsin digestion was performed at 37°C for 16 hrs, followed by freeze-drying of the samples.

7. Mass Spectrometry of Proteome

Dried peptides were dissolved in a 0.05% TFA solution. Five microliters of peptide samples were loaded onto a trapping column (Ultimate 3000 UPLC nanoviper Trap 5 μm Symmetry C_{18}, 100 μm x 20 mm) at a flow rate of 250 nL/min for 10 min. The analytical column used was a nanoviper (75 μm x 25 cm, NanoLC, Thermo Scientific, Waltham, MA, USA). Peptides were eluted at a flow rate of 250 nL/min over 80 min with a gradient of 0-45% acetonitrile. All MS and MS/MS spectra were acquired on a Q-Exactive Plus mass spectrometer (Thermo Fischer Scientific, Waltham, MA, USA) in data-dependent mode. Each full MS scan was performed in the range of 350-1900 *m/z*, and 12 of the most abundant precursor ion peaks were selected from the MS spectrum. MS/MS spectra were obtained by fragmenting each selected peak in data-dependent mode, and the electrospray voltage was set at 2.4 kV.

8. Protein Identification and Bioinformatics

The raw MS data were analyzed using MaxQuant software (version 1.5.3.17). MS/MS spectra were searched against the UniProt mouse database (www.uniprot.org, released in 2018.10, 59,345 entries) using the Andromeda search engine integrated into MaxQuant. Precursor and fragment ion mass tolerances were set to 5 and 25 ppm, respectively. Up to two mis-cleavages were allowed, and fixed carbamidomethylation (+57) and variable methionine oxidation (+16) were specified as fixed and variable protein modifications, respectively. Protein quantification analysis was performed by combining MS/MS spectra with the MaxQuant ion scoring approach for label-free quantitation. Peptides assigned with an FDR (false discovery rate) < 0.05 based on a threshold of $P < 0.05$ for individual ion scores were selected, and the analysis was performed using a mouse decoy database. Peptides were identified based on a single isotope mass, and the mass tolerances for precursor and fragment ions were both set to 25 ppm. Threshold scores and expected values for individual accepted spectra were based on the Mascot ion score threshold (0.05), and the calculated standard ion score thresholds for each

database search were followed.

Bioinformatics data analysis was performed based on MaxQuant analysis data using Perseus software (Tyanova et al., 2016). Relative protein quantification in the liver proteome was calculated by dividing the intensity of each original protein by the total intensity of all proteins in the sample through the entire protein frequency analysis. The resulting log2 values of the total protein intensity were scaled to appear as positive log2 values by arbitrarily multiplying them by 10^8. Annotations were categorized predominantly based on Gene Ontology (GO) Biological Processes (GOBP). Metabolic pathway mapping was represented in the KEGG (Kyoto Encyclopedia of Genes and Genomes) pathways in the form of UnitProt keywords. The relative protein abundance in the liver proteome of HFD-LNX mice compared to HFD mice and ND mice was analyzed in log2 scale. GO terms and KEGG pathways were displayed on each dataset using a two-dimensional enrichment analysis method (Cox and Mann, 2012). Hierarchical cluster analysis was performed using the Euclidean distance (Egami et al., 2021).

9. Comparison Analysis of DEPs and DEGs

To further investigate the differential expression patterns of DEPs and DEGs in response to normal diet vs. high-fat diet (HFD) and HFD vs. HFD with LNX supplementation, additional bioinformatics analysis was conducted. In order to assess the similarity between the expression patterns of proteins and transcripts, the Jaccard index was introduced (Chung et al., 2019). In summary, the Jaccard similarity index counts 1 when the expression pattern (increase or decrease) of a gene X is the same in both the mRNA and protein datasets, and 0 when it is different. The Jaccard similarity index (J_i) is represented as $a/(a+b+c)$ (where a indicates the concomitant increase or decrease of both mRNA and protein, and b and c indicate opposite changes in mRNA and protein, respectively). The similarity distance (J_d) is represented as $1 - a/(a+b+c)$. The modified Jaccard similarity index (J'_i) and similarity distance (J'_d) divide the degree of transcriptional and proteomic increase or decrease into intervals and are represented by multiplying a weighted factor of 0.6~1.0. Pearson's correlation was calculated to assess the correlation between the expression patterns of proteins and transcripts (Hack, 2004). For DEPs, the correlation of expression patterns with DEGs was determined using the Pearson correlation

R-value. The heat map was used to visually represent patterns where proteins and transcripts exhibited the same decrease or increase.

III. Results

1. Analysis of LNX Reveals Nectandrin B Predominantly

Mass spectrometry was employed for qualitative and quantitative analysis of the components of concentrated LNX extract. UV spectrum analysis revealed a main peak at a retention time of 7.85 min, identified as the ligand standard substance, nectandrin B (**Figure 2A**). Minor peaks were also observed, presumed to be other lignan components. In this experiment, other lignan standard compounds, aside from nectandrin B, were not available for preparation, and therefore, qualitative and quantitative analysis could not be conducted. The relative quantification of nectandrin B among the peaks in the entire UV spectrum confirmed it to be 82%. For precise structural analysis of nectandrin B, MS and MS/MS analyses were conducted (**Figure 2B, 2C**). Fragment ions derived from the sub-structure of nectandrin B were elucidated using CID, confirming its identity as nectandrin B.

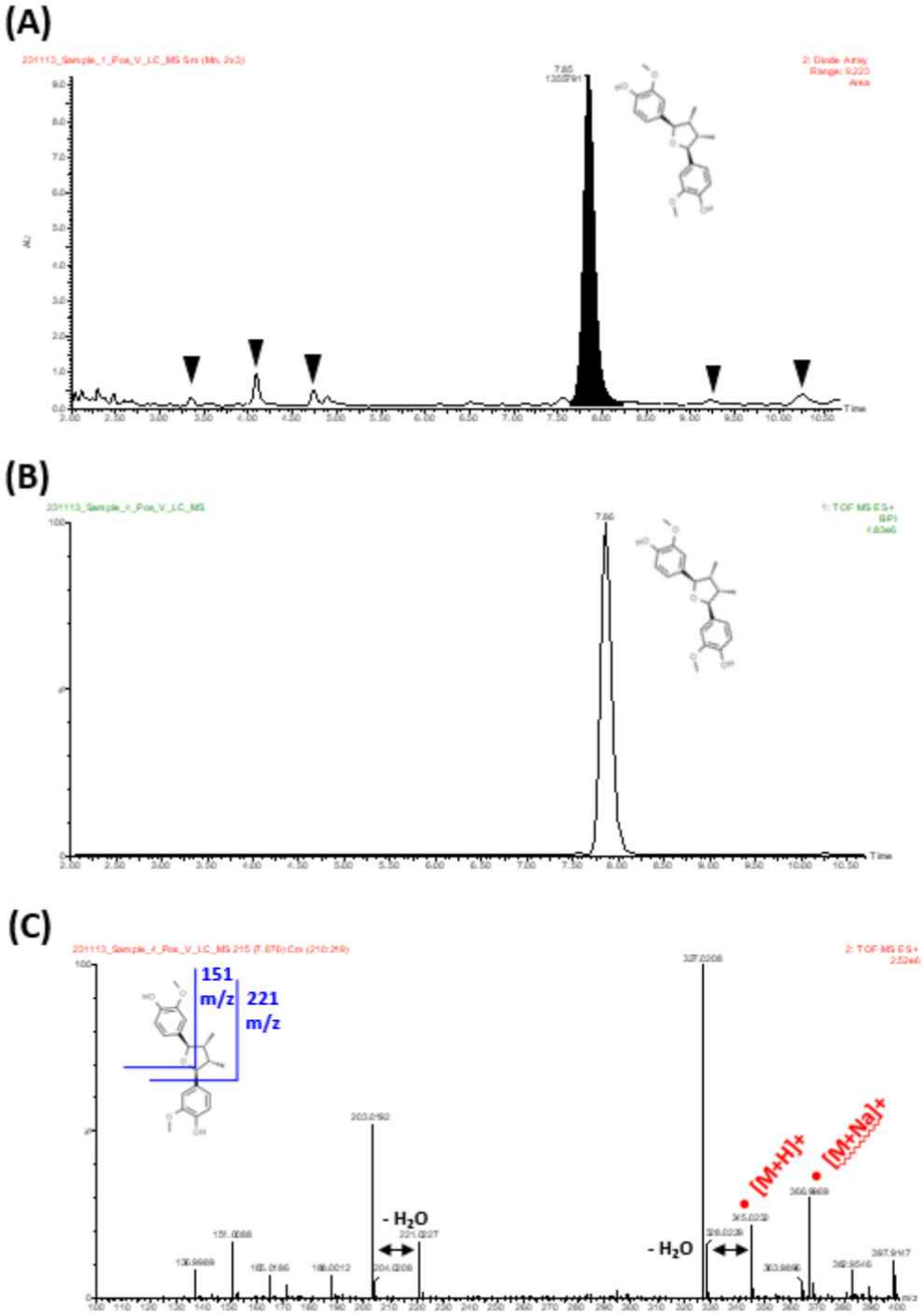

Figure 2. Analysis of nectandrin B content in LNX powder. UV spectrum of LNX mixture (A). Main peak at retention time (7.85 min) was identified as nectandrin B. Black triangles were suggested as minor lignans. MS spectrum (B) and MS/MS fragmentation (C) of nectandrin B were presented.

2. LNX Reduces Weight Gain in High-fat Diet Mice

HFD induced obesity symptoms in mice after 3 months compared to ND. HFD exhibited a 29% ($P<0.001$) increase in body weight at 3 months and a 26% increase at 6 months ($P<0.01$). However, when mice were fed LNX along with HFD, a 5% and 3% decrease was observed in low and high concentrations of LNX at 3 months, respectively, but statistically non-significant. Notably, at 6 months, low-concentration LNX showed a significant 9% decrease compared to HFD ($P<0.05$) (**Figure 3A**). Expressing weight loss as %Weight and Weight Gain, the anti-obesity effect of LNX was more pronounced. At 6 months, %Weight in mice fed low and high concentrations of LNX showed a 9% ($P<0.01$) and 6% ($P<0.05$) decrease, respectively (**Figure 3B**). Moreover, Weight Gain in mice fed low and high concentrations of LNX at 6 months exhibited a significant reduction of 24% ($P<0.001$) and 17% ($P<0.05$), respectively, compared to HFD (**Figure 3C**). To investigate if the cause of weight gain was related to food and water intake, the total amount consumed over 6 months was measured, showing no significant differences among groups (**Figure 4**).

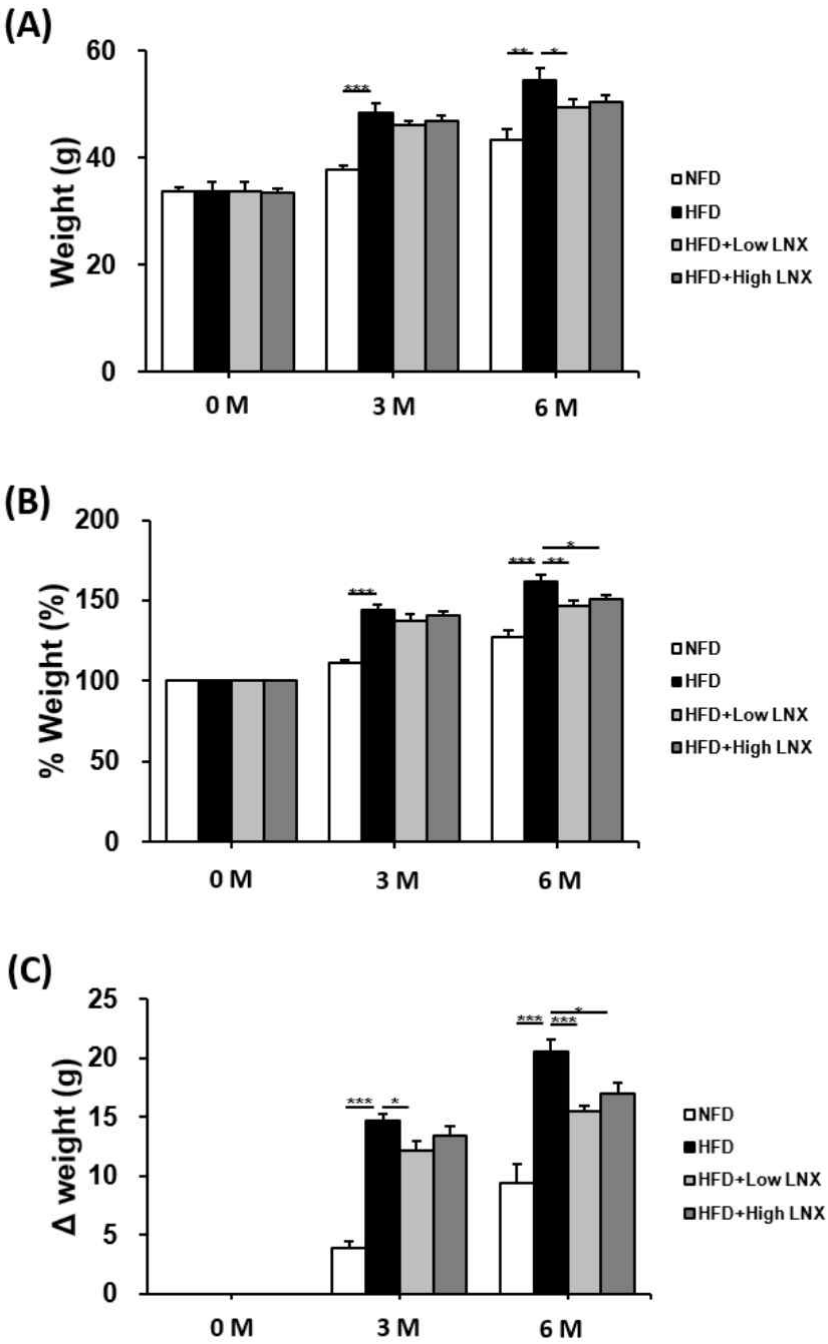

Figure 3. The change of body weight in experimental mice. At every 3 month (0, 3, 6 month), the body weight of mice was measured. Data of weight (A), % weight (B), weight gain (C) were presented as average ± SD. Statistical significance: $P < 0.05$ (*), $P < 0.01$ (**), $P < 0.001$ (***).

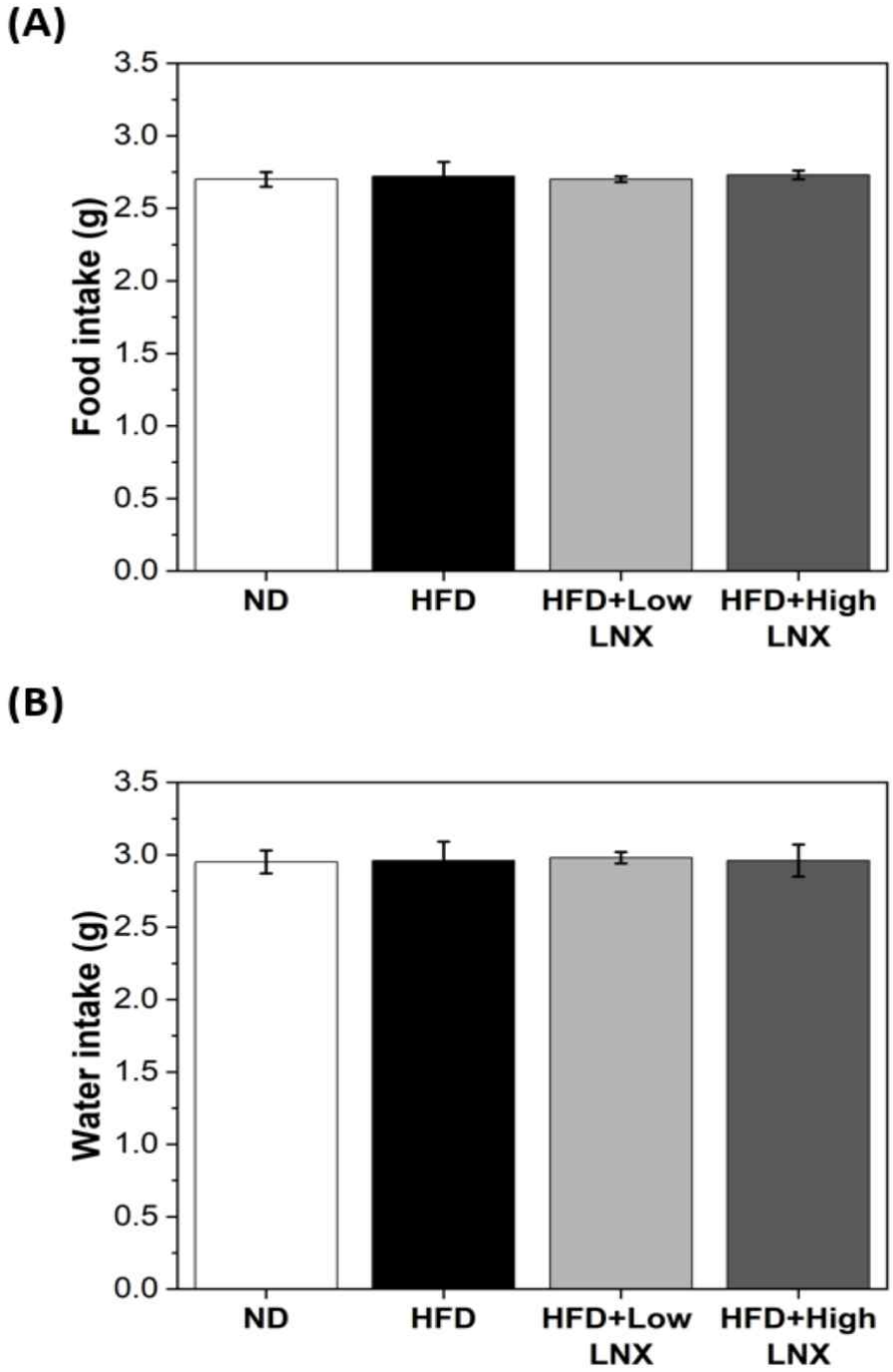

Figure 4. The change of food and water intake in experimental mice. At every 3 month (0, 3, 6 month), daily food (A) and water intake (B) was measured. Data were calculated as the daily consumption. Statistical significance: $P < 0.05$ (*), $P < 0.01$ (**), $P < 0.001$ (***).

3. LNX Reduces Elevated Blood Glucose and Triglycerides in High-fat Diet Mice

HFD induced a significant increase in blood glucose, total cholesterol, and HDL levels at 3 months compared to ND at $P<0.05$ (**Figure 5**). HFD showed a 55% increase in blood glucose at 3 months ($P<0.01$) and a 63% increase at 6 months ($P<0.001$). However, high-concentration LNX resulted in a 14% decrease at 3 months ($P<0.05$), and low-concentration LNX exhibited a 20% decrease at 6 months ($P<0.001$) compared to HFD (**Figure 5A**). Although low-concentration LNX at 3 month and high-concentration LNX at 6 month showed the decreased pattern compared to control, both cases didn't show any statistical significance. While no significant difference was observed in triglycerides between ND and HFD, both concentrations of LNX significantly reduced triglycerides by 25% ($P<0.01$) and 31% ($P<0.05$) at 3 and 6 months, respectively (**Figure 5B**). Total cholesterol and HDL showed a significant increase in HFD compared to ND at $P<0.05$, but LNX, although exhibiting a slight increase compared to HFD, did not reach significance (**Figure 5C-E**).

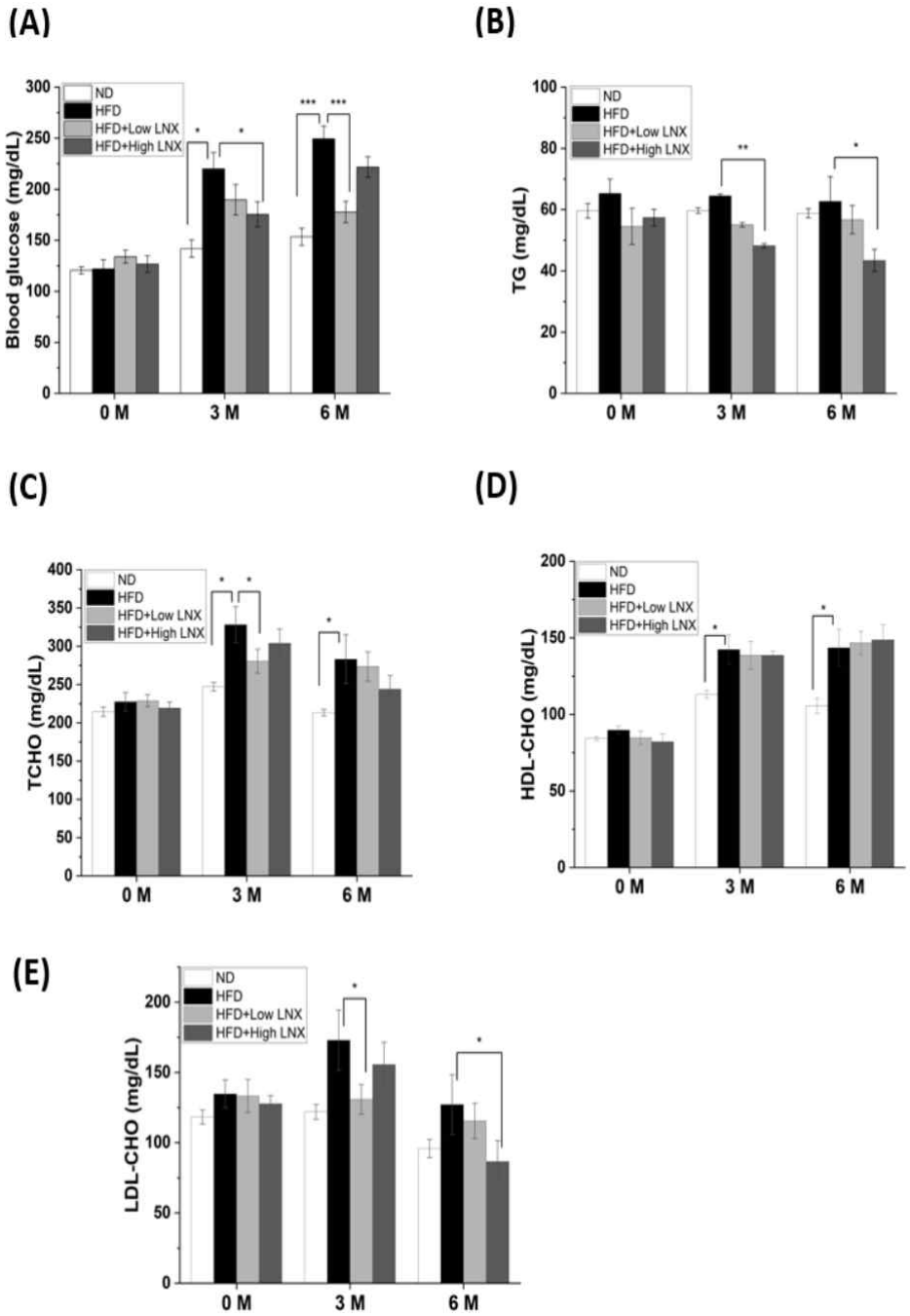

Figure 5. The change of blood glucose, neutral lipid and cholesterol in mice. At every 3 month (0, 3, 6 month), blood sample was extracted to analyze blood glucose (A), triglyceride (B), total cholesterol (C), HDL-cholesterol (D), and LDL-cholesterol (E). Data were presented as average ± SD. Statistical significance: $P < 0.05$ (*), $P < 0.01$ (**), $P < 0.001$ (***).

4. LNX Reduces Increased Body Fat in High-fat Diet Mice

To further investigate the weight loss induced by LNX in HFD, body composition was analyzed through whole body imaging. Mice were scanned with DEXA at different time points and conditions. HFD, compared to ND, showed a noticeable increase in volume at 3 and 6 months, with excessive accumulation of internal fat components (red region) (**Figure 6**). However, when mice were fed LNX along with HFD, a decrease was observed at 6 months, especially with high-concentration LNX showing a significant reduction compared to HFD. This was quantitatively analyzed by distinguishing weight, fat, lean mass, and fat percentage (**Figure 7**). Body weight increased significantly in HFD compared to ND at 3 and 6 months, with a 31% and 27% increase, respectively ($P<0.001$). Both low and high concentrations of LNX resulted in a 12% decrease compared to HFD at 6 months ($P<0.05$) (**Figure 7A**). Fat showed a substantial increase of 108% and 80% in HFD compared to ND at 3 and 6 months, respectively ($P<0.001$). Low and high concentrations of LNX resulted in a 24% ($P<0.001$) and 17% ($P<0.01$) decrease at 3 months, and at 6 months, a 17% ($P<0.001$) and 36% ($P<0.01$) decrease, respectively (**Figure 7B**). Lean mass, in contrast, increased by 17% in low-concentration LNX compared to HFD at 3 months ($P<0.05$) and by 23% in high-concentration LNX compared to HFD at 6 months ($P<0.05$) (**Figure 7C**). Fat percentage increased significantly in HFD compared to ND at 3 and 6 months, with a 58% and 42% increase, respectively ($P<0.001$). Low-concentration LNX resulted in a 12% decrease at 3 months ($P<0.01$), and high-concentration LNX showed a 28% decrease at 6 months ($P<0.001$) (**Figure 7D**).

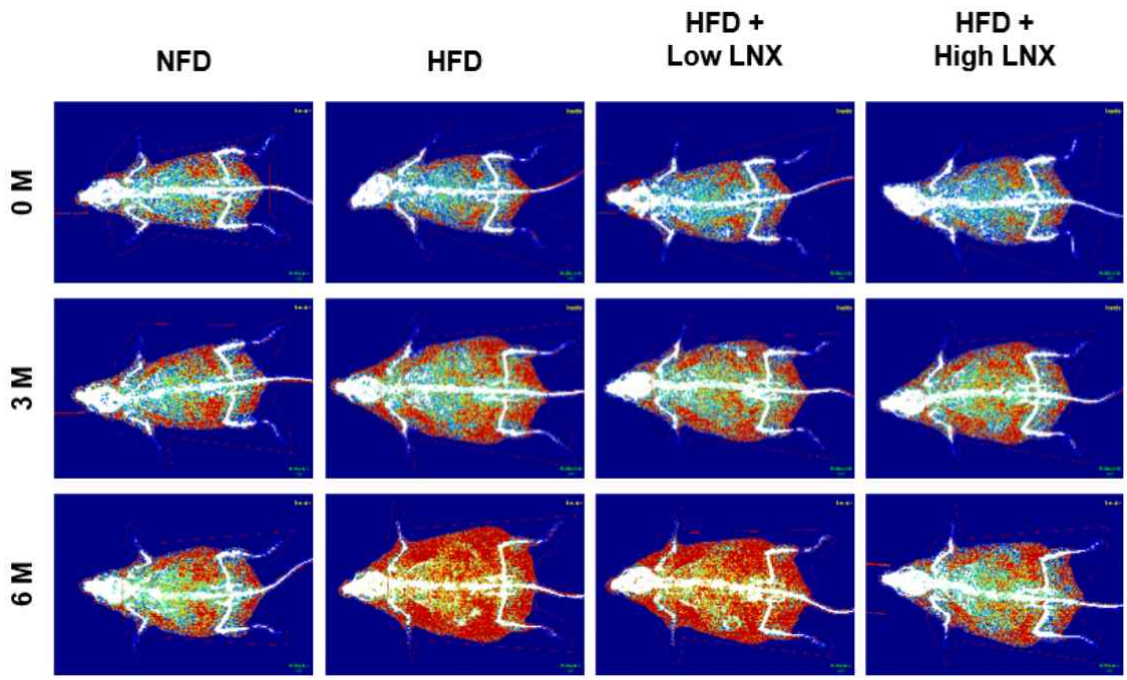

Figure 6. DEXA analysis of body fat and bone in experimental mice. At every 3 month (0, 3, 6 month), whole body of experimental mice were photographed and measured by DEXA. Image analysis procedure was described in detail in Materials and Methods. The whole body images of body fat (red region) and body bone (white region) as a typical sample were clearly distinguished each other.

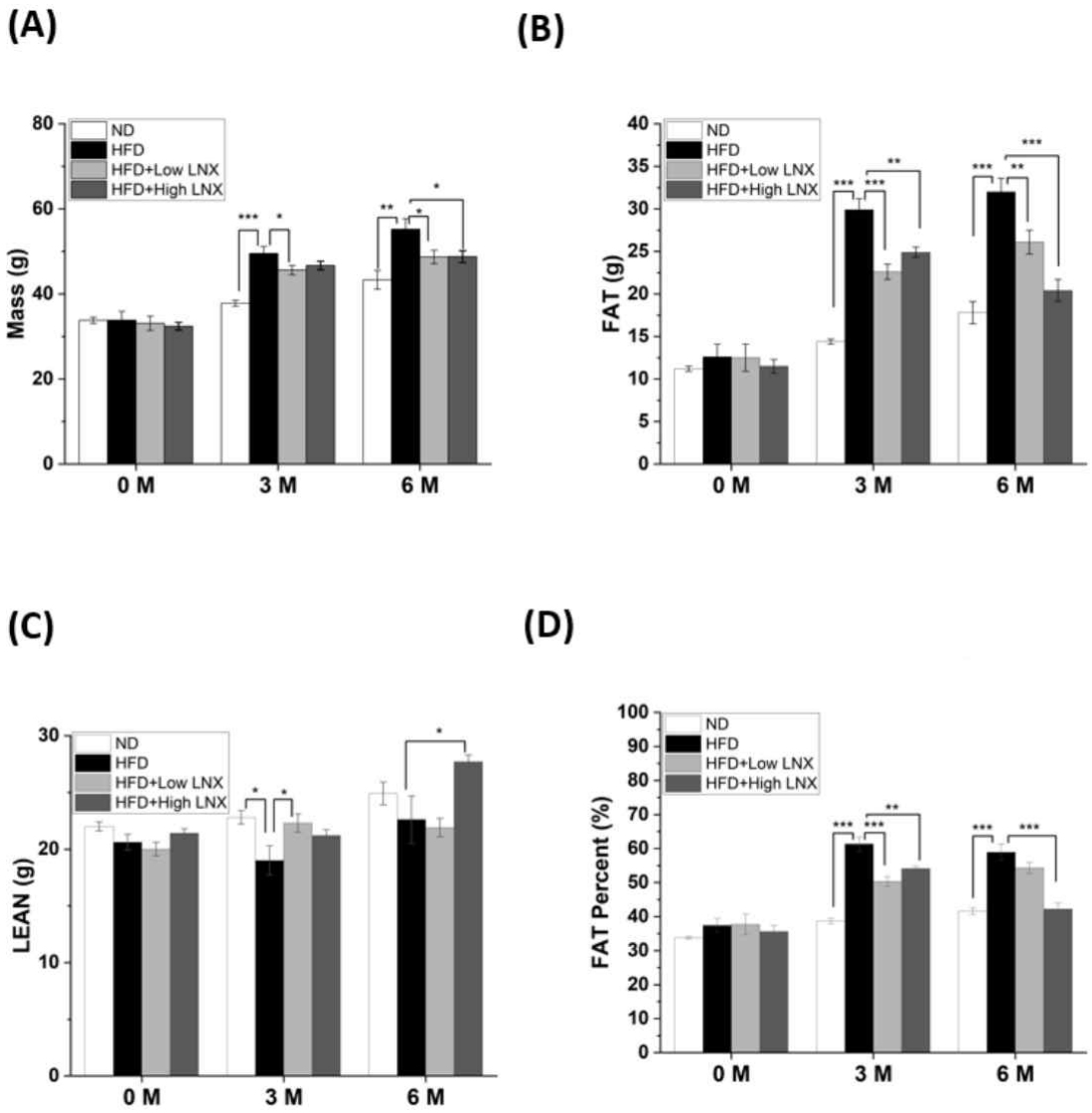

Figure 7. DEXA analysis of body mass and fat in experimental mice. At every 3 month (0, 3, 6 month), DEXA analysis of whole body was conducted to measure mass (A), fat (B), lean (C), and fat % (D) from each group. Data were presented as average ± SD. Statistical significance: $P < 0.05$ (*), $P < 0.01$ (**), $P < 0.001$ (***).

5. LNX Reduces Bone Density Increased by High-fat Diet Mice

Whole-body scans by DEXA can provide information about bones. Investigation of bone mineral content (BMC), bone mineral density (BMD), and bone area and volume was conducted for mouse bones affected by HFD and LNX. There was no observed change in BMC between ND and HFD or between HFD and LNX (**Figure 8A**). However, BMD increased significantly in HFD compared to ND, showing a 24% increase at 3 months and 19% at 6 months ($P<0.001$). In contrast, low-concentration LNX decreased by 12% at 3 months ($P<0.01$) and 8% at 6 months ($P<0.001$), while high-concentration LNX decreased by 11% at both 3 and 6 months ($P<0.05$) (**Figure 8B**). Conversely, bone area exhibited results opposite to BMD. HFD showed a 12% decrease at 3 months ($P<0.01$) and a 14% decrease at 6 months, although not statistically significant. Low-concentration LNX increased by 19% at 3 months and 16% at 6 months compared to HFD ($P<0.05$). High-concentration LNX increased by 17% at 3 months and 28% at 6 months ($P<0.01$) (**Figure 8C**). However, there were no significant differences in bone volume among all groups (**Figure 8D**).

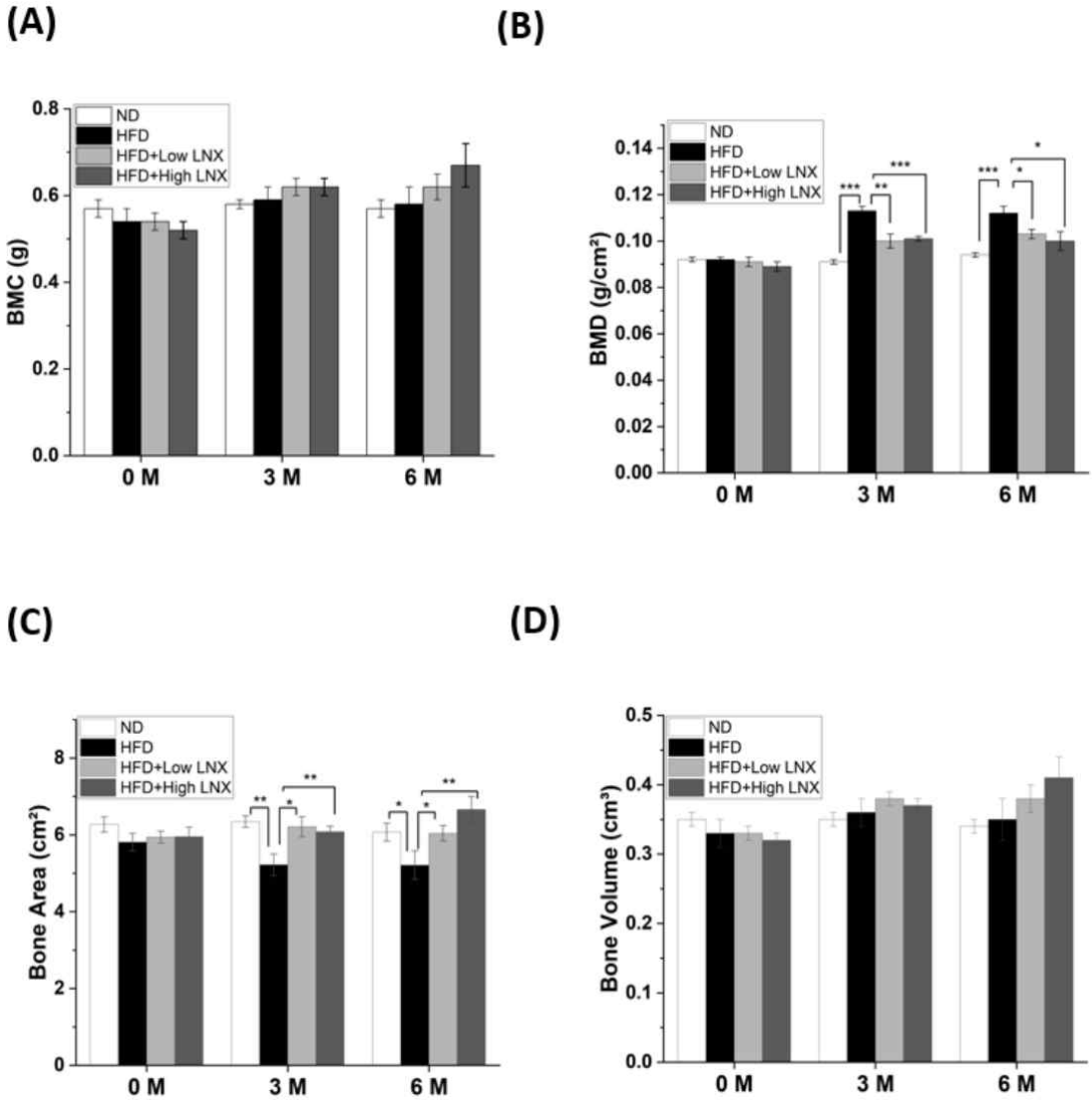

Figure 8. DEXA analysis of bone in experimental mice. At every 3 month (0, 3, 6 month), DEXA analysis of whole body was conducted to measure bone mineral content (A), bone mineral density (B), bone area (C), and bone volume (D) from each group. Data were presented as average ± SD. Statistical significance: $P < 0.05$ (*), $P < 0.01$ (**), $P < 0.001$ (***).

6. LNX Suppresses Fat Accumulation in Mouse Liver and Adipose Tissues

To quantitatively investigate the relative increase in hepatic fat induced by HFD and how much fat accumulated in the liver and adipose tissue, a thorough examination was conducted. Over 6 months, HFD visibly accumulated fat in the liver (**Figure 9A**). Quantitative analysis of hepatic fat accumulation showed a 158% increase in HFD compared to ND ($P<0.001$), but low-concentration LNX with HFD did not result in a significant change compared to HFD (9% increase, not statistically significant), and high-concentration LNX with HFD led to a remarkable 31% decrease compared to HFD ($P<0.01$) (**Figure 9B**). Additionally, examining adipocytes from intestinal tissues revealed that the adipocyte diameter increased by 88% in HFD compared to ND ($P<0.001$), whereas low and high concentrations of LNX with HFD resulted in a 37% and 42% decrease, respectively ($P<0.001$) (**Figure 9C**). Adipocyte area also showed an increase of 207% in HFD compared to ND ($P<0.001$), while low and high concentrations of LNX with HFD led to a 48% and 54% decrease, respectively ($P<0.001$) (**Figure 9D**).

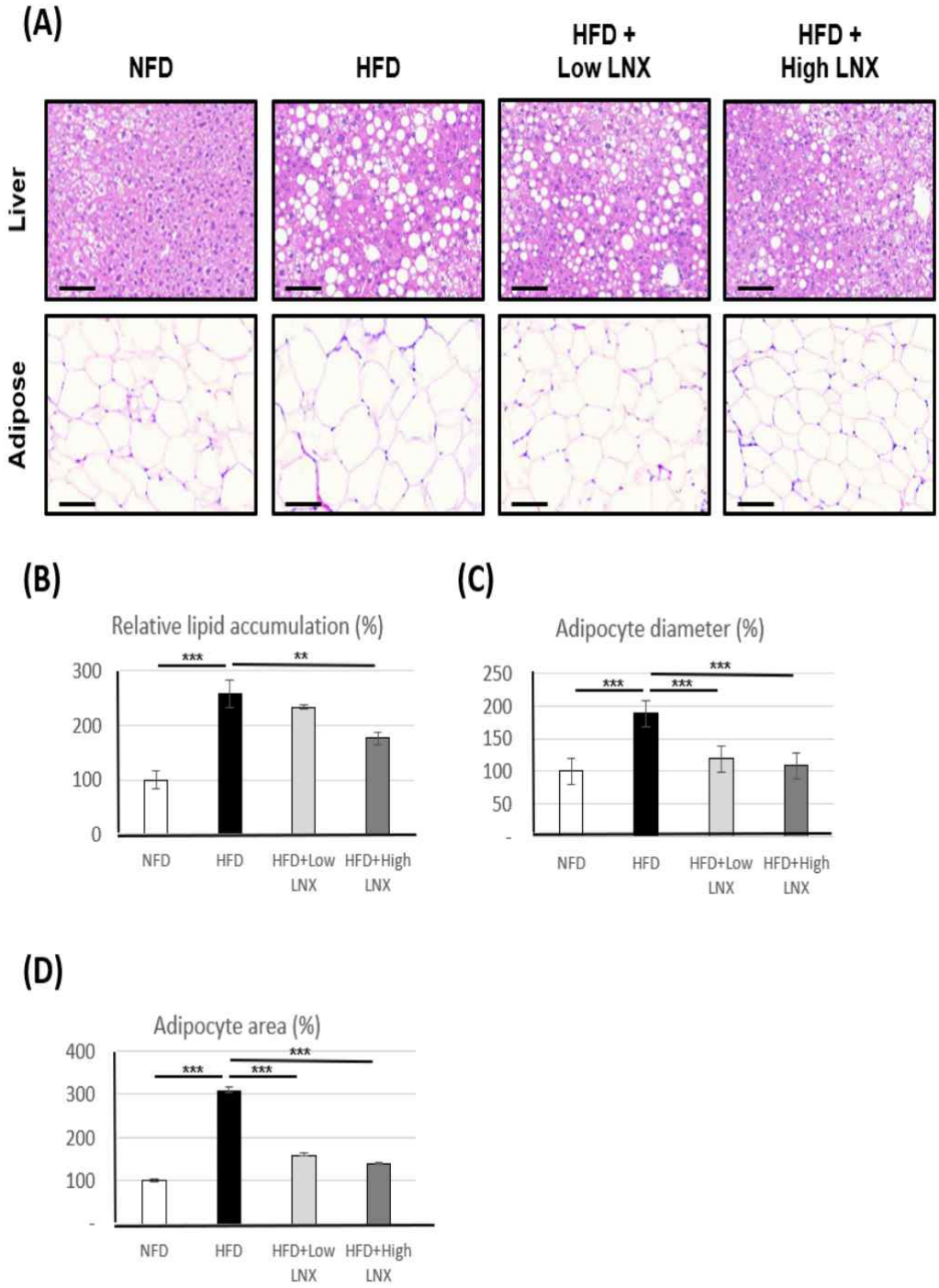

Figure 9. Histology and H&E staining of liver and adipose tissue in mice. At final 6 month, the experimental mice were sacrificed to extract liver and adipose tissues. H&E staining of liver and adipose tissue (A) was quantified as relative lipid accumulation% (B), adipocyte diameter% (C), and adipocyte area% (D). Data were presented as average ± SD. Statistical significance: , $P < 0.01$ (**), $P < 0.001$ (***).

7. LNX Modulates Hepatic Proteins in HFD Mice

To explore possible anti-obesity proteins induced by LNX in HFD-induced obese mice, liver proteins were analyzed using label-free proteomic analysis. Proteins were isolated from liver tissues of each experimental animal, separated by SDS-PAGE, subjected to in-gel tryptic digestion, and identified by a high-sensitivity Q-Exactive-Plus mass spectrometer. The shotgun proteomic analysis revealed 20,208, 19,807, and 18,164 peptides identified in ND, HFD, and LNX-HFD groups, respectively (**Table 2**). The total proteins identified were 2,020 in ND, 1,875 in HFD, and 1,994 in LNX-HFD. A Venn diagram analysis showed that 1,893 proteins were commonly identified among three experimental groups, covering 77-87% of the proteome in each group (**Figure 10**). Exclusive protein identifications were 181 (8.3%) in ND, 209 (8.5%) in HFD, and 35 (1.6%) in LNX-HFD.

Correlations between individual samples were investigated based on their unique protein expression patterns. The heat map analysis of the overall protein expression data showed that samples within the ND group exhibited a perfect 100% correlation, while samples within the HFD and LNX-HFD groups showed 89% and 80% correlations, respectively (**Figure 11**). Thus, the high-fat diet demonstrated distinct protein pattern differences from the normal diet, and LNX consumption showed 11~20% inter-individual variability. In addition, clustering analysis of individual protein expression patterns between groups was conducted (**Figure 12**). ND group samples were completely separated into distinct clusters, and both HFD and LNX-HFD groups displayed separate cluster patterns. Both HFD and LNX-HFD groups further divided into two subgroups.

Cluster heat map and volcano plot analyses were performed to identify differentially expressed proteins (DEPs) between HFD and ND (**Figure 13**). A total of 936 DEPs were identified using the criteria of $P<0.05$ and fold change >1.5. Among these, 593 proteins were up-regulated, and 343 proteins were down-regulated in response to the high-fat diet. Similar analyses were conducted for DEPs between LNX-HFD and HFD. Heat map clustering analysis revealed distinct patterns of protein expression changes induced by LNX (**Figure 14A**), and there were 180 DEPs including 52 up-regulated and 128 down-regulated DEPs by LNX (**Figure 14B**).

Table 2. Numbers of identified proteins

Group	Peptides	Unique Peptides	Proteins*	MS/MS Count
ND (n=4)	24,549 ±1,357	20,208 ±1,140	2,020 ±61	61,455 ±4,200
HFD (n=9**)	24,099 ±2,498	19,807 ±2,128	1,875 ±144	53,283 ±6,548
LNX-HFD (n=10)	22,149 ±2,594	18,164 ±2,209	1,994 ±126	46,477 ±6,119

*Proteins were identified by UniProt mouse database (www.uniprot.org, released in 2018.10, 59,345 entries) with unique peptides.

**Initially 10 mice were started in HFD group but one mouse was dead during the experiment.

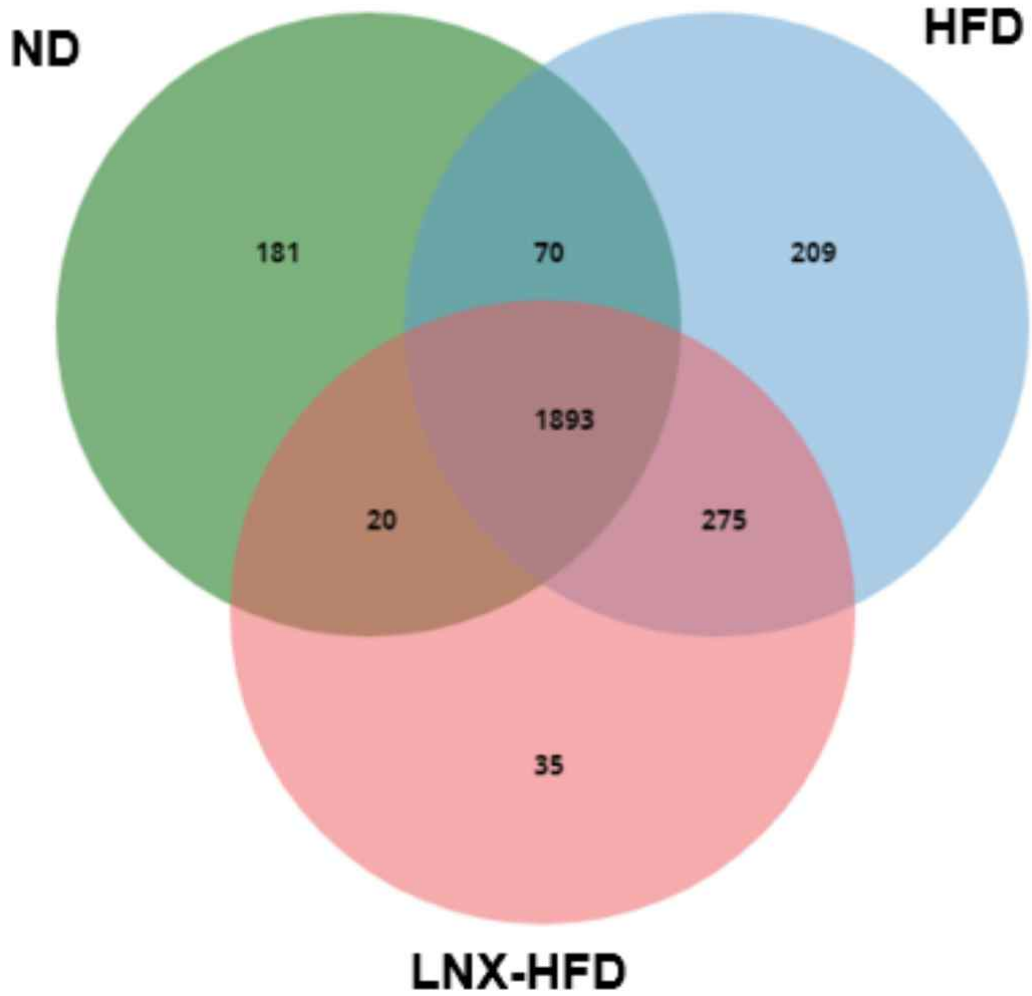

Figure 0. Venn diagram of identified mouse hepatic proteins. Total proteins belonged to each group was collected with shared peptides of homologous proteins. Sample number : ND (n=4), HFD (n=9), LNX-HFD (n=10).

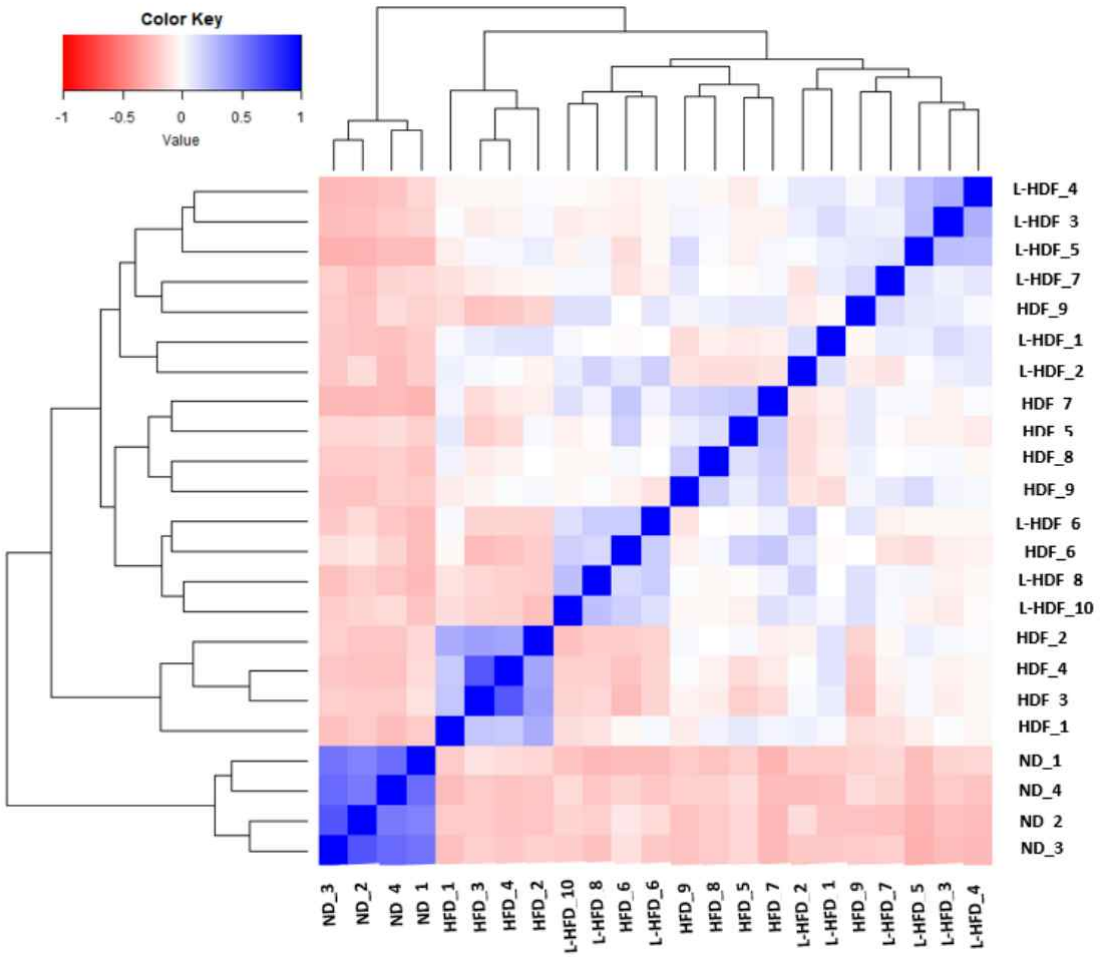

Figure 11. Sample-to-sample correlation heat map of mouse hepatic proteomes. Diagonal blue box indicates the similarity values colored as blue.

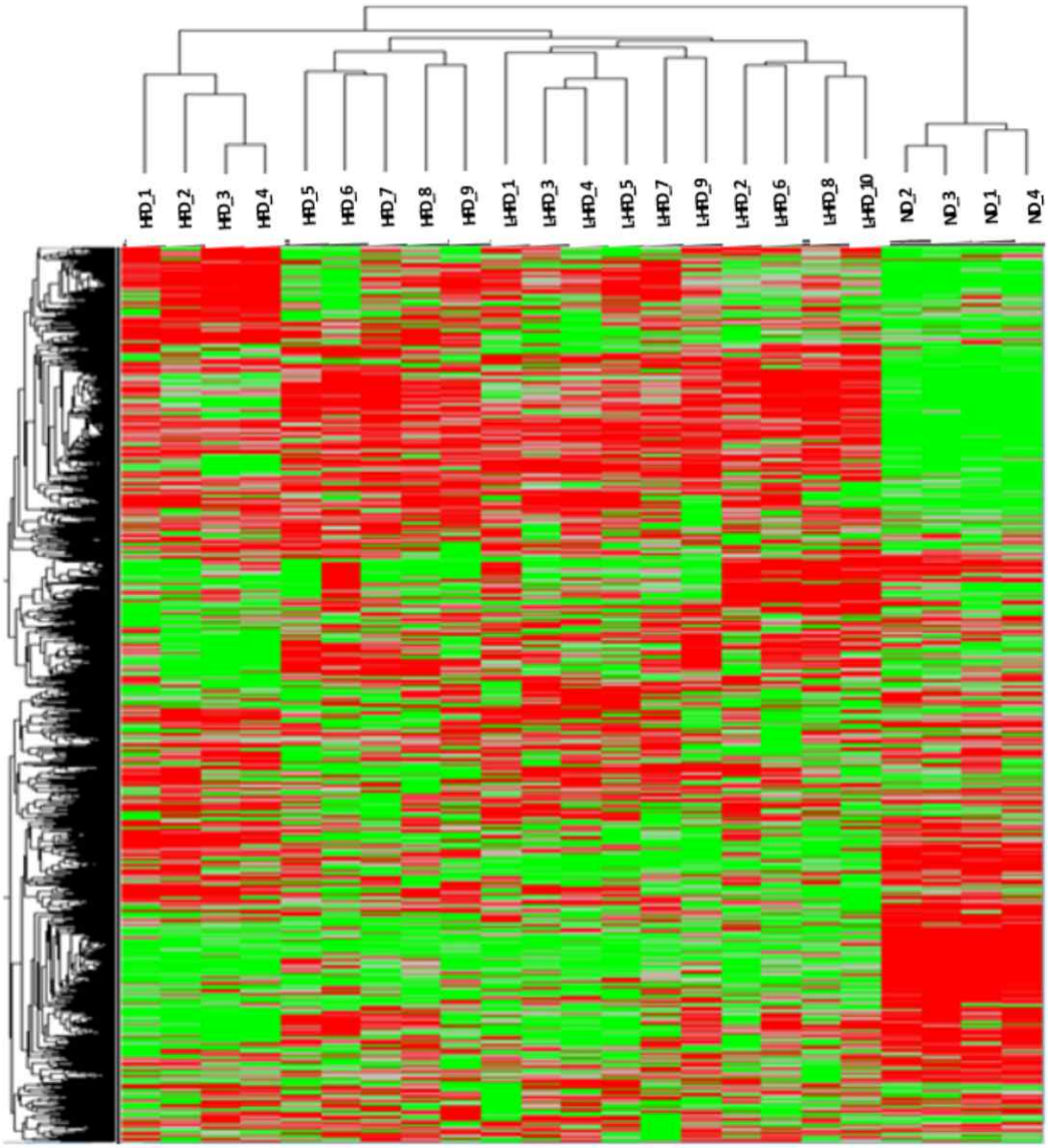

Figure 12. Hierarchical clustering of individual mouse hepatic proteomes. Red and green bars indicate the up and down-regulated proteins (HFD/ND or LNX-HFD/HFD), respectively.

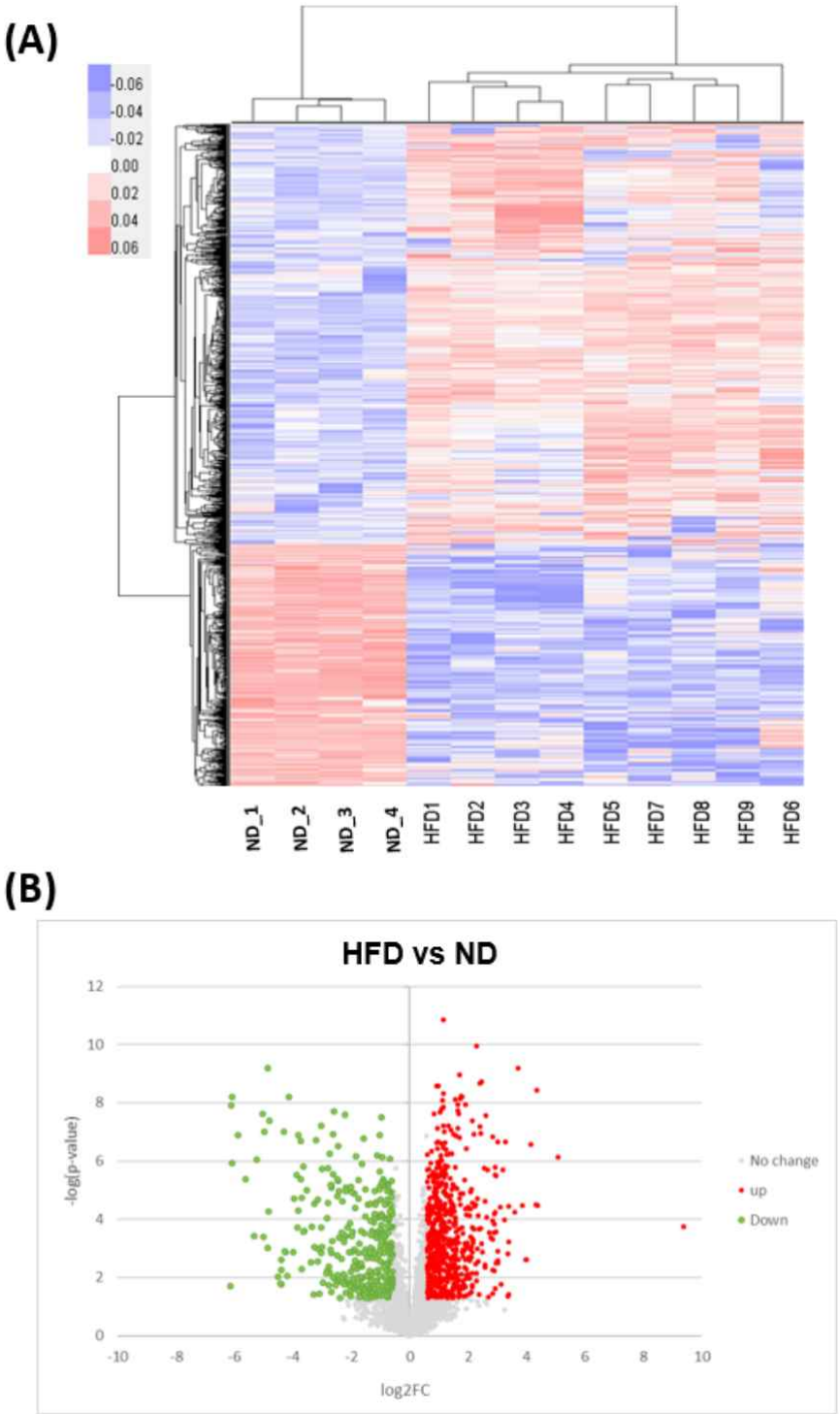

Figure 13. Heat map and volcano plot of mouse hepatic proteomes in HFD/ND. Hierarchical clustering of proteins were presented by heat map (A) and volcano plot (B) of up (red) and down-regulated proteins (green) selected by the threshold ($P<0.05$, fold change>1.5). Proteome data were selected by the criterion at FDR < 0.05.

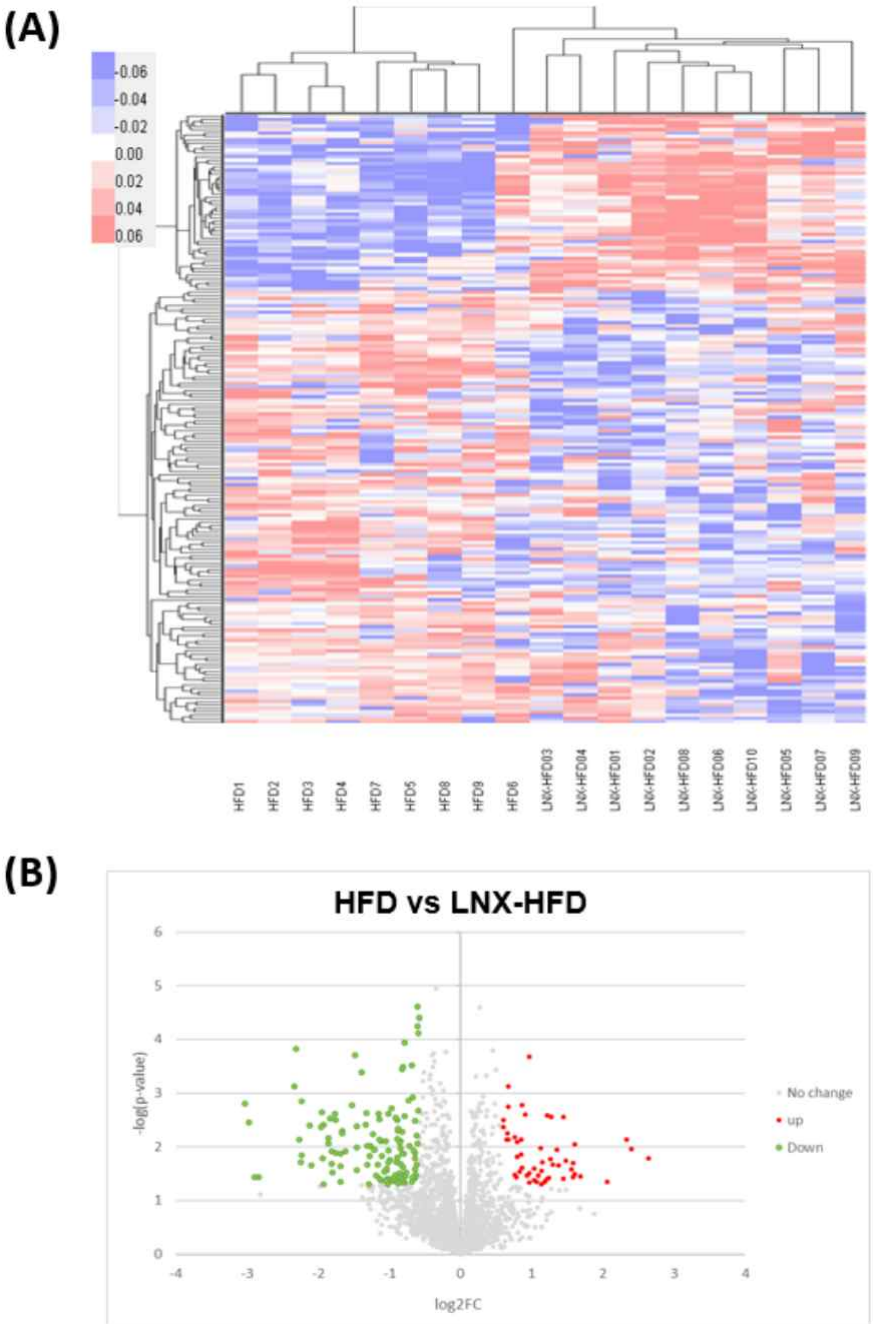

Figure 14. Heat map and volcano plot of mouse hepatic proteomes in LNX-HFD/HFD. Hierarchical clustering of proteins were presented by heat map (A) and volcano plots (B) of up (red) and down-regulated proteins (green) selected by the threshold ($P<0.05$, fold change>1.5). Proteome data were selected by the criterion at FDR < 0.05.

For a more focused analysis, proteins were categorized based on their expression reversal by LNX, specifically those that increased with obesity in HFD and decreased with LNX (or *vice versa*). Using the same criteria as for transcriptomes ($P<0.05$, fold change >1.5), a summary of these proteins is presented in **Table 3**. The results indicated that LNX increased 11 proteins that were decreased by obesity and decreased 42 proteins that were increased by obesity. Notably, proteins involved in lipid and fatty acid metabolism, as well as those related to immune and defense mechanisms, were prominently affected by LNX, revealing its impact on biological processes related to obesity (**Figure 15**). When DEPs were categorized by Biological Process, proteins up-regulated by LNX were predominantly associated with translation and lipid metabolism (**Figure 16**), whereas proteins down-regulated by LNX were mainly involved in metabolic processes, mitochondrial function, and immune response (**Figure 16**).

Table 3. List of DEPs regulated by LNX

				HFD / ND		LNX-HFD / HFD	
ID	GN	BP	Description	P-value	FC	P-value	FC
Q8K4Z3	Naxe	Lipid metabolism	NAD(P)H-hydrate epimerase	0.046	-1.66	0.006	1.58
P62849	Rps24	Translation	40S ribosomal protein S24	0.036	-8.53	0.011	5.31
Q8BP67	Rpl24	Translation	60S ribosomal protein L24	0.033	-4.52	0.039	2.73
P25444	Rps2	Translation	40S ribosomal protein S2	0.028	-1.69	0.002	1.59
P14115	Rpl27a	Translation	60S ribosomal protein L27a	0.016	-21.55	0.017	6.25
P12970	Rpl7a	Translation	60S ribosomal protein L7a	0.012	-5.46	0.018	2.78
A0A140LIT2	Dhcr7	Lipid metabolism	7-dehydrocholesterol reductase	0.011	-3.54	0.003	2.73
P62918	Rpl8	Translation	60S ribosomal protein L8	0.008	-2.48	0.007	1.81
A0A1L1SVK0	Pafah1b2	Lipid metabolism	Platelet-activating factor acetylhydrolase IB subunit alpha2 (Fragment)	0.007	-7.27	0.007	5.06
P62900	Rpl31	Translation	60S ribosomal protein L31	0.000	-2.45	0.000	1.96
O09111	Ndufb11	Mitochondrial function	NADH dehydrogenase [ubiquinone] 1 beta subcomplex subunit 11, mitochondrial	0.000	-8.97	0.038	2.36
Q8R3F5	Mcat	Fatty acid metabolism	Malonyl-CoA-acyl carrier protein transacylase, mitochondrial	0.047	1.94	0.003	-2.21
O55229	Chkb	Fatty acid metabolism	Choline/ethanolamine kinase	0.046	2.15	0.047	-1.72
Q5RL20	Mrpl43	Mitochondrial function	39S ribosomal protein L43, mitochondrial	0.044	2.40	0.038	-1.93
P17918	Pcna	DNA replication	Proliferating cell nuclear antigen	0.044	3.22	0.042	-2.07
A2AWT6	Ubtf	Transcription	Nucleolar transcription factor 1	0.043	2.10	0.005	-1.84
Q04207	Rela	Transcription	Transcription factor p65	0.042	2.78	0.042	-2.00
G5E8R2	Tpm1	Cytoskeleton	Tropomyosin alpha-1 chain	0.037	1.65	0.000	-2.80
P62774	Mtpn	Metabolic process	Myotrophin	0.037	7.07	0.003	-7.83
Q5F2F2	Abhd15	Lipid metabolism	Protein ABHD15	0.036	1.64	0.013	-1.76
F6QN75	Lman2l	Immune response	VIP36-like protein (Fragment)	0.036	2.06	0.003	-1.84
A0A1L1SR69	Higd1a	Mitochondrial function	HIG1 domain family member 1A, mitochondrial (Fragment)	0.027	2.79	0.015	-2.43
Q91WK5	Gcsh	Mitochondrial function	Glycine cleavage system H protein, mitochondrial	0.021	3.23	0.006	-3.17
Q9WTL7	Lypla2	Fatty acid metabolism	Acyl-protein thioesterase 2	0.019	4.37	0.012	-3.51
P60060	Sec61g	Translocation	Protein transport protein Sec61 subunit gamma	0.013	4.84	0.023	-3.22
Q9D8S9	Bola1	Mitochondrial function	BolA-like protein 1	0.012	2.42	0.009	-1.65
A0A0R4IZZ5	Clec4f	Immune response	C-type lectin domain family 4 member F	0.008	1.63	0.009	-1.52
Q8VE88	Fam114a2	Metabolic process	Protein FAM114A2	0.008	2.68	0.000	-2.61
Q9DB60	Prxl2b	Lipid metabolism	Prostamide/prostaglandin F synthase	0.008	3.06	0.007	-2.21
Q91XL9	Osbpl1a	Lipid metabolism	Oxysterol-binding protein-related protein 1	0.008	3.36	0.040	-2.20
E9Q7Q3	Tpm3	Cytoskeleton	Tropomyosin alpha-3 chain	0.007	1.53	0.000	-1.61
Q91VB8	Hba-a1	Defense response	Alpha globin 1	0.005	2.22	0.005	-1.76
P26883	Fkbp1a	Metabolic process	Peptidyl-prolyl cis-trans isomerase FKBP1A	0.003	7.73	0.004	-3.88
Q8VD31	Tapbpl	Immune response	Tapasin-related protein	0.002	2.03	0.030	-1.70
A0A494BBP6	Nt5c2	Defense response	Cytosolic purine 5'-nucleotidase	0.002	2.63	0.012	-2.02
Q0P688	Eif4e2	Translation	Eukaryotic translation initiation factor 4E member 2	0.002	4.35	0.019	-2.02
Q8R050	Gspt1	Translation	Eukaryotic peptide chain release factor GTP-binding subunit ERF3A	0.001	1.77	0.002	-2.22
Q6ZWY3	Rps27l	Translation	40S ribosomal protein S27-like	0.001	1.99	0.000	-1.52
A0A0N4SVB8	Arl8b	Protein transport	ADP-ribosylation factor-like protein 8B	0.001	4.92	0.000	-1.77
Q8BUK6	Hook3	Protein transport	Protein Hook homolog 3	0.001	2.00	0.003	-1.88
P01887	B2m	Immune response	Beta-2-microglobulin	0.000	2.15	0.002	-1.51
Q9QYA2	Tomm40	Mitochondrial function	Mitochondrial import receptor subunit TOM40 homolog	0.000	7.70	0.045	-3.22
P52503	Ndufs6	Mitochondrial function	NADH dehydrogenase [ubiquinone] iron-sulfur protein 6, mitochondrial	0.000	1.63	0.000	-1.52
P68033	Actc1	Metabolic process	Actin, alpha cardiac muscle 1	0.000	1.72	0.000	-1.77
A8DUK4	Hbb-bs	Defense response	Beta-globin	0.000	3.48	0.022	-1.53
P31725	S100a9	Immune response	Protein S100-A9	0.000	12.13	0.010	-2.74
Q5RKZ7	Mocs1	Metabolic process	Molybdenum cofactor biosynthesis protein 1	0.000	2.00	0.045	-1.61
Q8R1Q9	Rbks	Metabolic process	Ribokinase	0.000	2.70	0.004	-2.52
Q9R092	Hsd17b6	Lipid metabolism	17-beta-hydroxysteroid dehydrogenase type 6	0.000	5.88	0.002	-1.95
Q8BTZ7	Gmppb	Metabolic process	Mannose-1-phosphate guanyltransferase beta	0.000	2.13	0.050	-2.03
Q7TNG5	Eml2	Cytoskeleton	Echinoderm microtubule-associated protein-like 2	0.000	33.55	0.049	-3.80
A0A2R8VHF9	Myh11	Cytoskeleton	Myosin-11	0.000	9.71	0.000	-7.04
Q91WK2	Eif3h	Translation	Eukaryotic translation initiation factor 3 subunit H	0.000	8.03	0.042	-2.16

*Red colored proteins (Clec4f, S100a9, Hsd17b6) were shown as the similar expression pattern in transcriptomic analysis. See Figure 28.

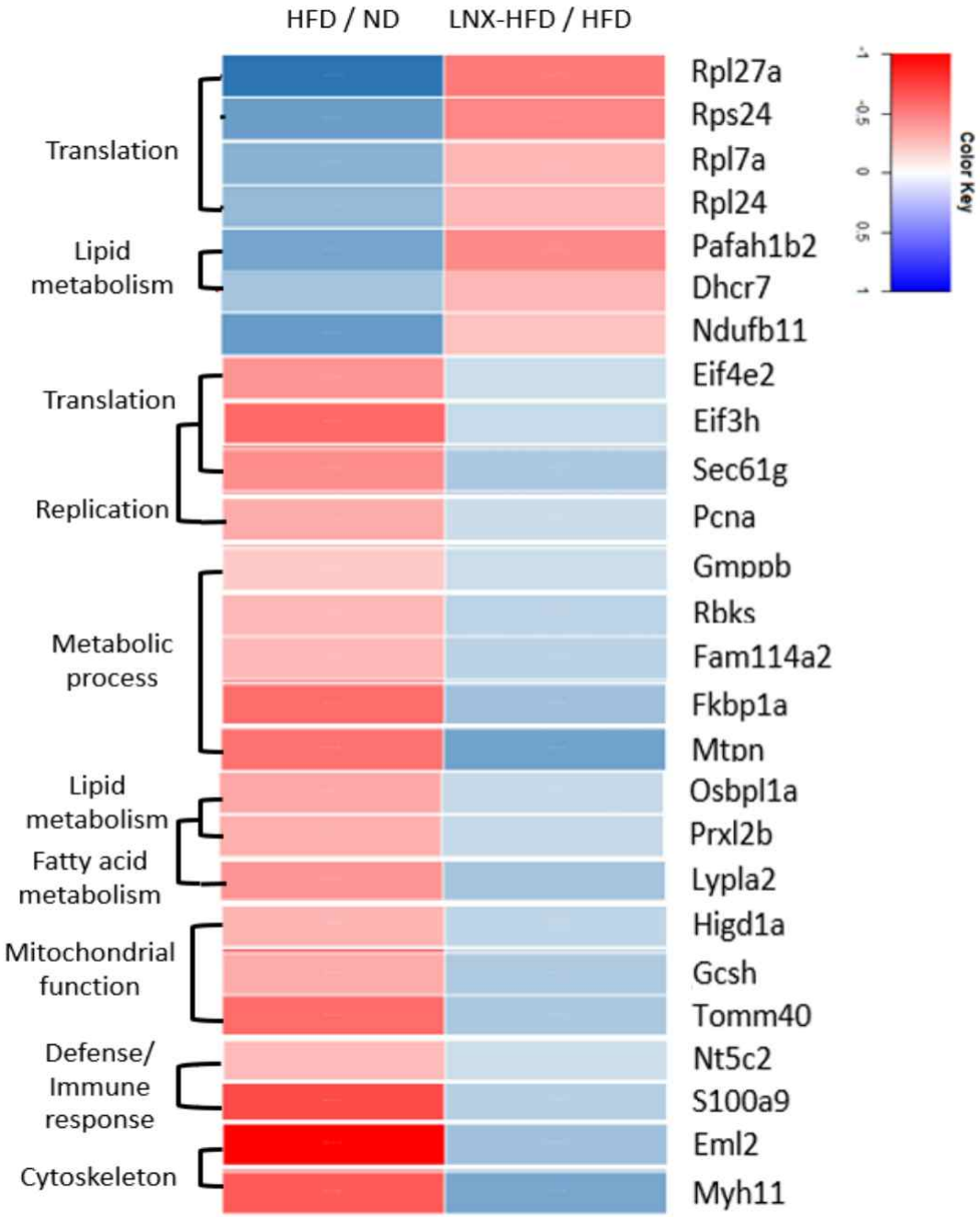

Figure 15. Functionally clustered heat map of LNX target proteins. Two groups are divided into Group I (LNX-induced up-regulation of decreased proteins by HFD) and Group II (LNX-induced down-regulation of increased proteins by HFD). Color intensity of red and blue indicates up and down-regulation degree, respectively. Sample number : ND (n=4), HFD (n=9), LNX-HFD (n=10).

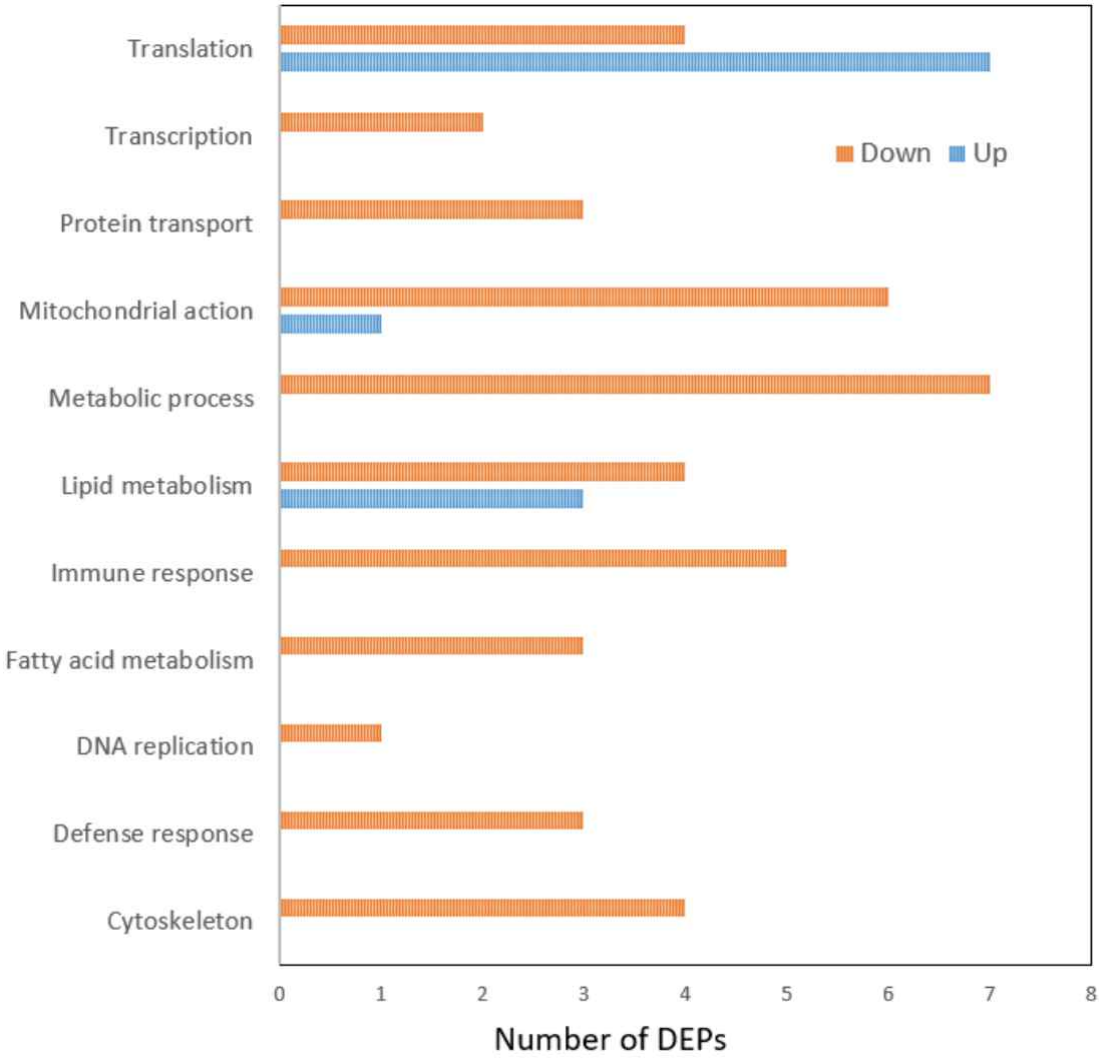

Figure 16. Classification of LNX target proteins by functional category. DEPs were classified by down (orange) and up (blue)-regulated proteins by LNX. DEPs were selected by the criterion, FDR < 0.05. Sample number : ND (n=4), HFD (n=9), LNX-HFD (n=10).

8. LNX Modulates Hepatic Transcriptome in HFD Mice

To investigate the transcriptional changes induced by a high-fat diet (HFD) in obese mice and the anti-obesity effects of LNX, RNA-Seq was employed to analyze the hepatic transcriptome. The Venn diagram in **Figure 17A** illustrates commonly expressed transcripts between HFD and ND as well as between LNX-HFD and HFD. A total of 1,161 differentially expressed genes (DEGs) were identified out of 23,183 genes analyzed. Of these DEGs, 535 were up-regulated, and 613 were down-regulated in response to HFD compared to ND (**Figure 17B, 17C**). Among the DEGs that were either up-regulated or down-regulated in response to HFD and exhibited a reverse trend in LNX-HFD, 13 genes were identified. These genes met the criteria of a fold change greater than 1.5, an average normalized data (Log2) above 2, and a P-value less than 0.05.

A total of 13 target genes regulated by LNX were identified under the specified conditions. The heat map in **Figure 18** displays clusters of genes whose expression is reversed by LNX, with 6 genes up-regulated and 7 genes down-regulated. Genes up-regulated by LNX included Cyp51, Fdps, Gm40794, Sqle, Cyp26b1, and Thrsp, associated with cholesterol synthesis, lipid metabolism, and bone formation. Genes down-regulated by LNX included Cbr2, Dbp, Cyp7a1, LOC118567333 (Gm25018), Ciart, Krt23, and Rg4, involved in carbohydrate metabolism, circadian rhythm regulation, hormone synthesis, epithelial cell differentiation, and GPCR signaling. The total number of transcripts identified was 10,859 for HFD/ND and 10,707 for LNX-HFD/HFD. The volcano plot in **Figure 19A** visually represents these transcripts based on fold change and P-value. Additionally, scatter plots in **Figure 19B** separate transcripts with a fold change greater than 1.5 in HFD/ND and LNX-HFD/HFD. The 13 target genes identified under LNX discovery conditions are marked as outliers beyond the baseline.

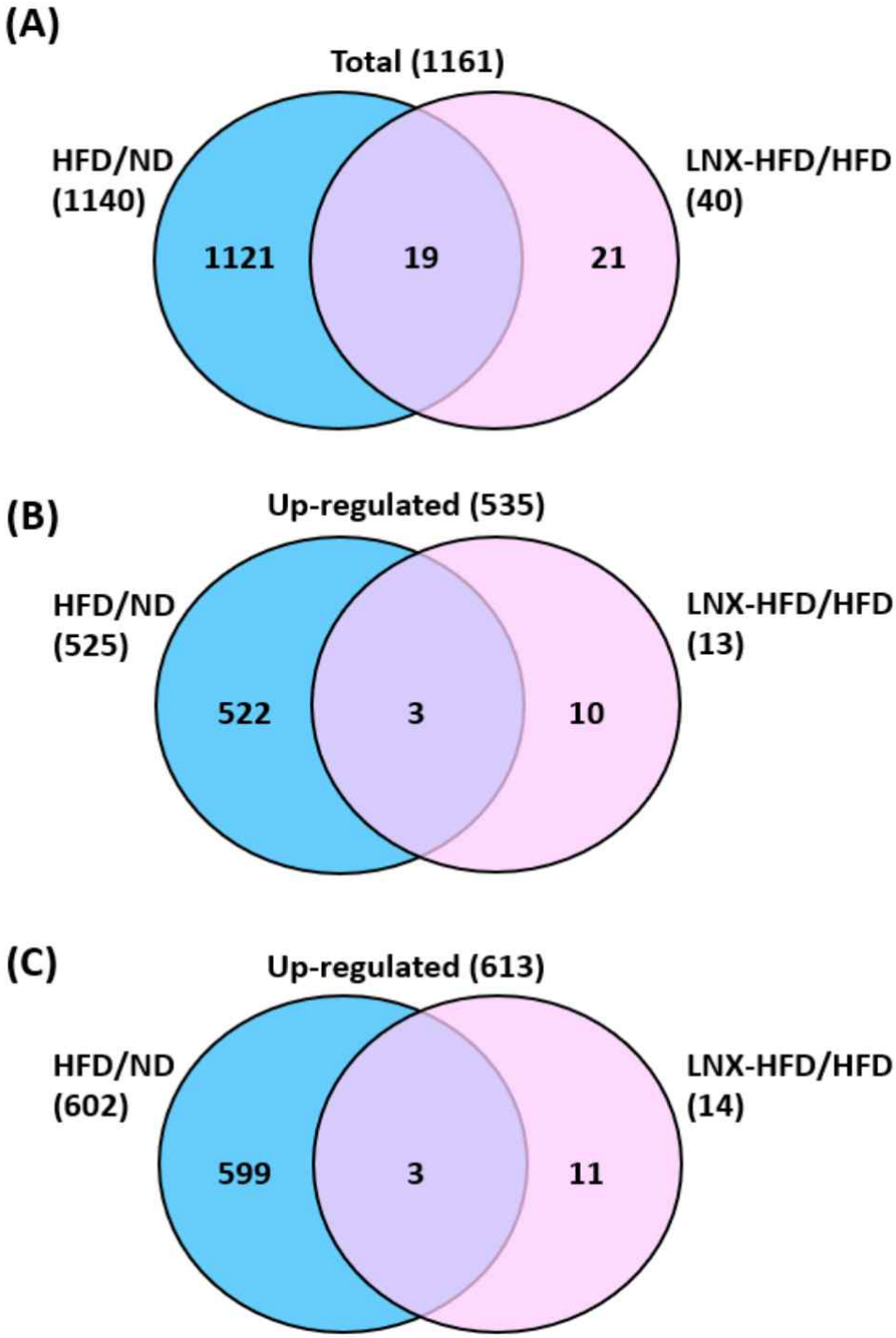

Figure 17. Venn diagram of identified mouse hepatic transcripts. A total of transcripts (1161) were identified in ND, HFD, LNX-HFD groups (A). DEGs were classified by 535 up-regulated (B) and 613 down-regulated transcripts (C).

(A)

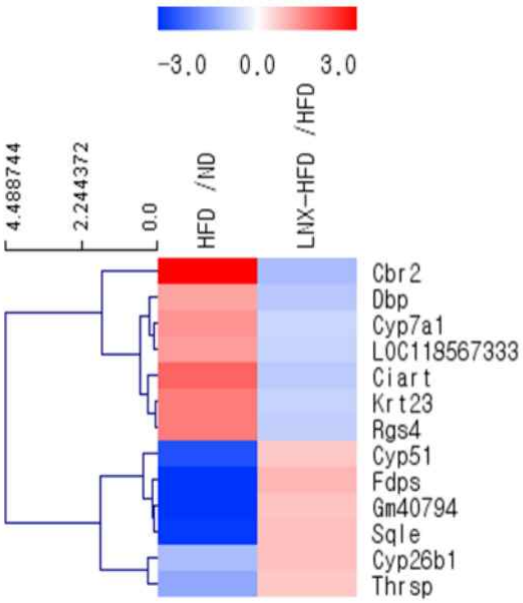

(B)

Gene	Protein	Category	Fold-change
Up-regulated genes by LNX in obesity condition			
Cyp51	Lanosterol 14-alpha demethylase	Cholesterol biosynthesis	1.576
Fdps	Farneyl pyrophosphate synthase	Cholesterol biosynthesis	1.801
Gm40794	-		1.624
Sqle	Squalene monooxygenase	Cholesterol metabolic process	1.676
Cyp26b1	Cytochrome P450 26B1	Bone morphogenesis	1.669
Thrsp	Thyroid hormone-inducible hepatic protein	Lipid metabolic process	1.561
Down-regulated genes by LNX in obesity condition			
Cbr2 (AP27)	Carbonyl reductase 2	Glucose metabolism	-1.957
Dbp	D site-binding protein	Circadian rhythm	-1.757
Cyp7a1	Steroid 17-alpha-hydroxylase/17,20 lyase	Hormone biosynthetic process	-1.511
LOC118567333	-		-1.563
Ciart	Circadian-associated transcriptional repressor	Circadian regulation	-1.695
Krt23	Keratin, type I cytoskeletal 23	Epithelial cell differentiation	-1.563
Rgs4	Regulator of G-protein signaling 4	GPCR signaling pathway	-1.616

Figure 18. Clustering heat map of LNX target genes. Thirteen LNX target genes are presented as clustering map (A). List of target genes are presented in the table (B). After transcriptome analysis, gene code was extracted from genome alignment. LNX target genes were selected by the threshold of $P<0.05$ and $FC>1.5$. Gm40794 and LOC118567333 were considered as hypothetical proteins.

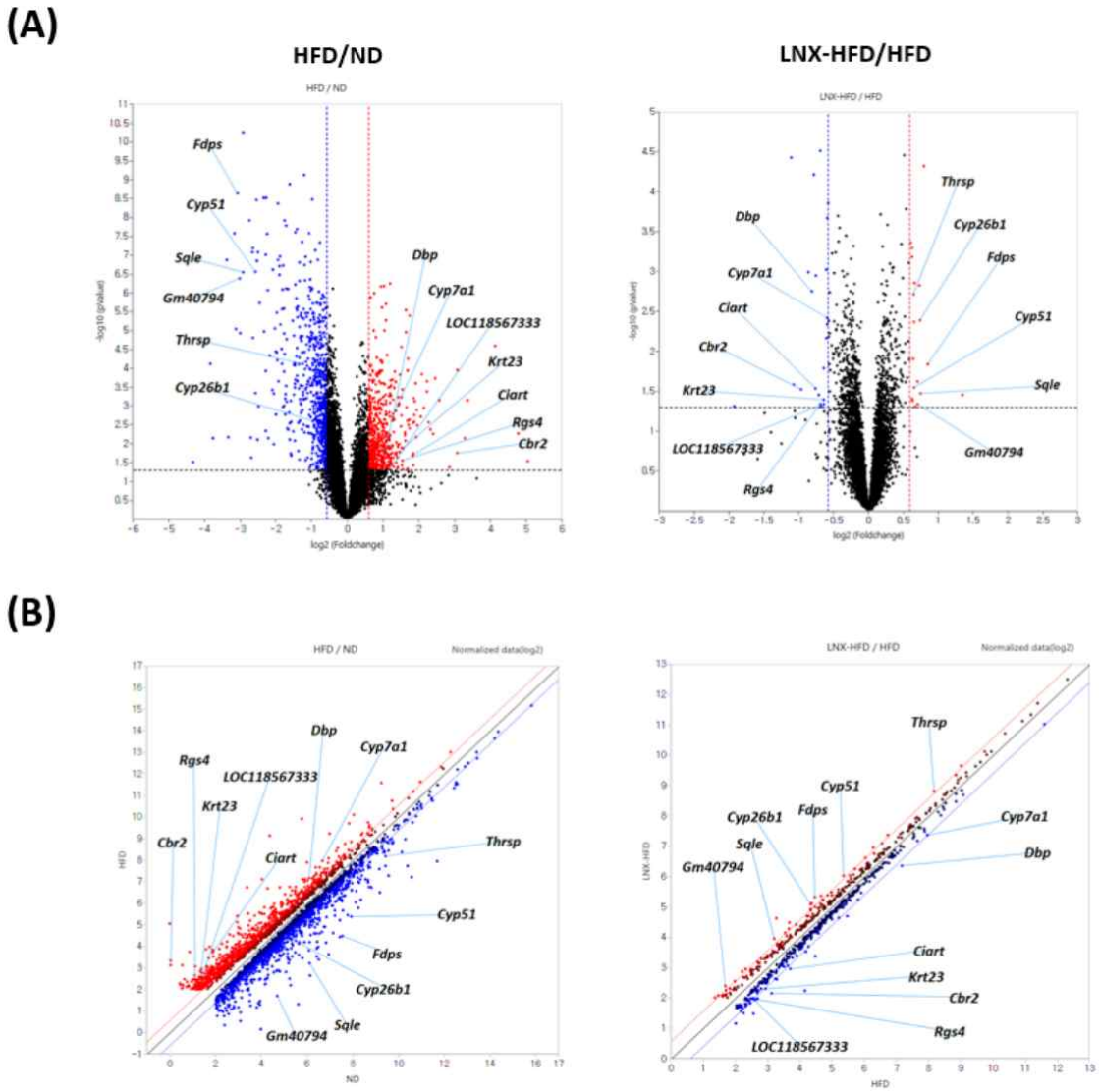

Figure 19. Volcano and scatter plots of total transcripts. The identified transcripts in either HFD or ND (10,859) and in either LNX-HFD or HFD (10,707) were displayed as volcano plot showing fold change and P-value (A). Dotted line means the P-value less than 0.5. The identified transcripts between HFD and ND (2,917) and between LNX-HFD and HFD (670) were displayed as scatter plot showing fold change (B). Diagonal lines mean the fold change greater than 1.5.

Gene Ontology (GO) analysis of the identified DEGs revealed the functional categories enriched in the comparison of HFD/ND and LNX-HFD/HFD. In the HFD/ND comparison, the up-regulated genes were associated with lipid metabolism (73 genes), fatty acid metabolism (31 genes), carbohydrate metabolism (17 genes), and alcohol metabolism (17 genes) (**Figure 20A**). The down-regulated genes were associated with lipid metabolism (105 genes), fatty acid metabolism (43 genes), and alcohol metabolism (38 genes). In the LNX-HFD/HFD comparison, the up-regulated genes were associated with lipid metabolism (5 genes), alcohol metabolism (3 genes), and gluconeogenesis (1 gene), while the downregulated genes were associated with carbohydrate metabolism (3 genes), lipid and alcohol metabolism (1 gene) (**Figure 20B**).

Further classification of DEGs into Gene Ontology Biological Processes (GOBP) provided insight into the top 10 categories based on P-value for both HFD/ND and LNX-HFD/HFD (**Figure 21**). In HFD/ND, lipid metabolism, fatty acid metabolism, and steroid metabolism were highly expressed, while in LNX-HFD/HFD, cholesterol metabolism, fatty acid metabolism, and steroid metabolism were top-ranked by confidence. The representation of data for the top 10 categories of GOBP in terms of P-value and fold enrichment (FE) is shown in **Figure 22**. In HFD/ND, lipid metabolism, fatty acid metabolism, and steroid metabolism exhibited high P-values, but FE was not high. Sterol biosynthetic processes showed the highest FE (**Figure 22A**). In LNX-HFD/HFD, cholesterol metabolism, lipid metabolism, and sterol metabolism displayed high P-values, whereas bile acid biosynthesis and circadian rhythm regulation showed high FE (**Figure 22B**).

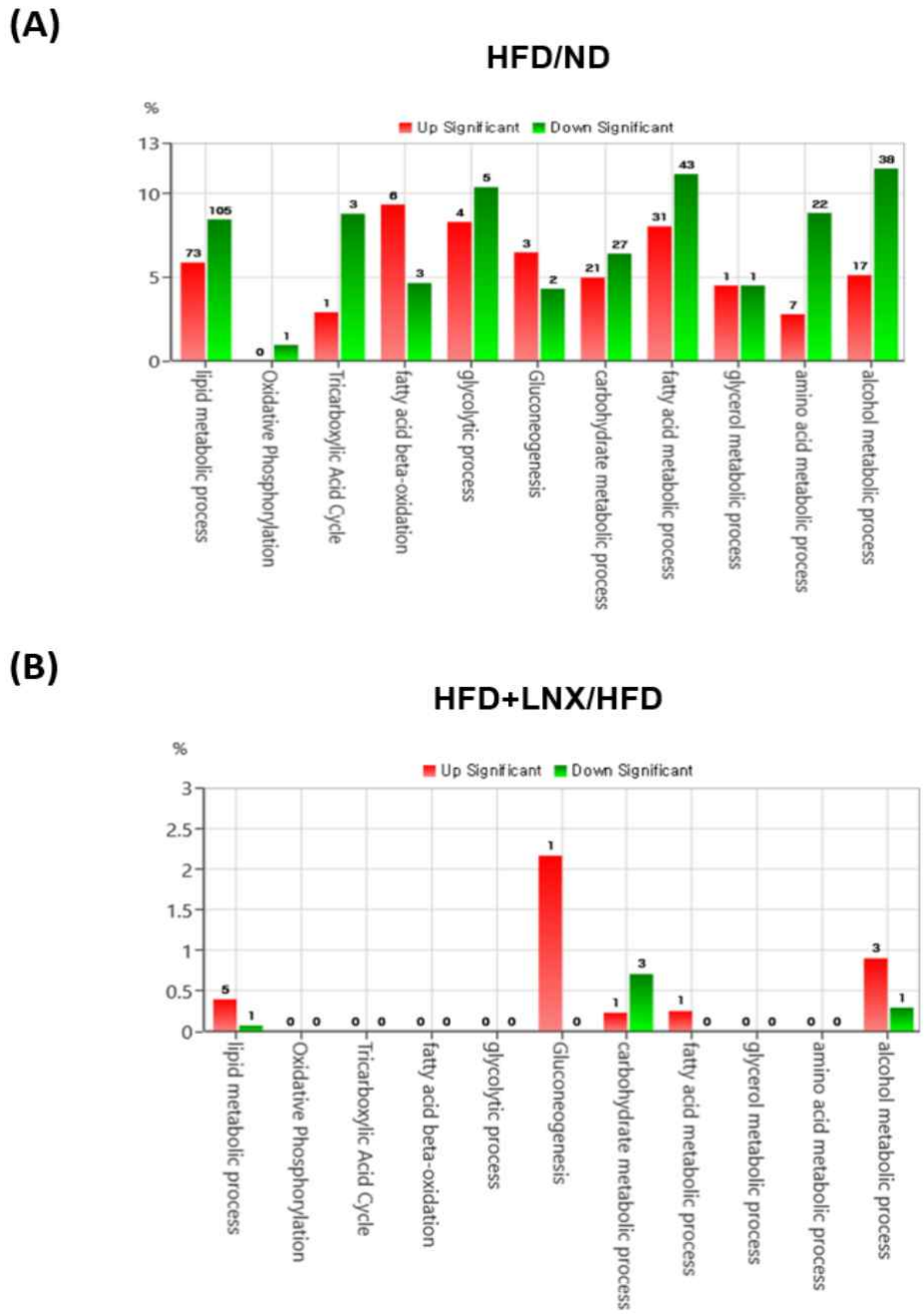

Figure 20. Gene ontology analysis of mouse hepatic DEGs. DEGs in HFD compared to ND (A) and HFD-LNX compared to HFD (B) were displayed by biological category. Red and green bar indicates up-regulated and down-regulated transcript, respectively .

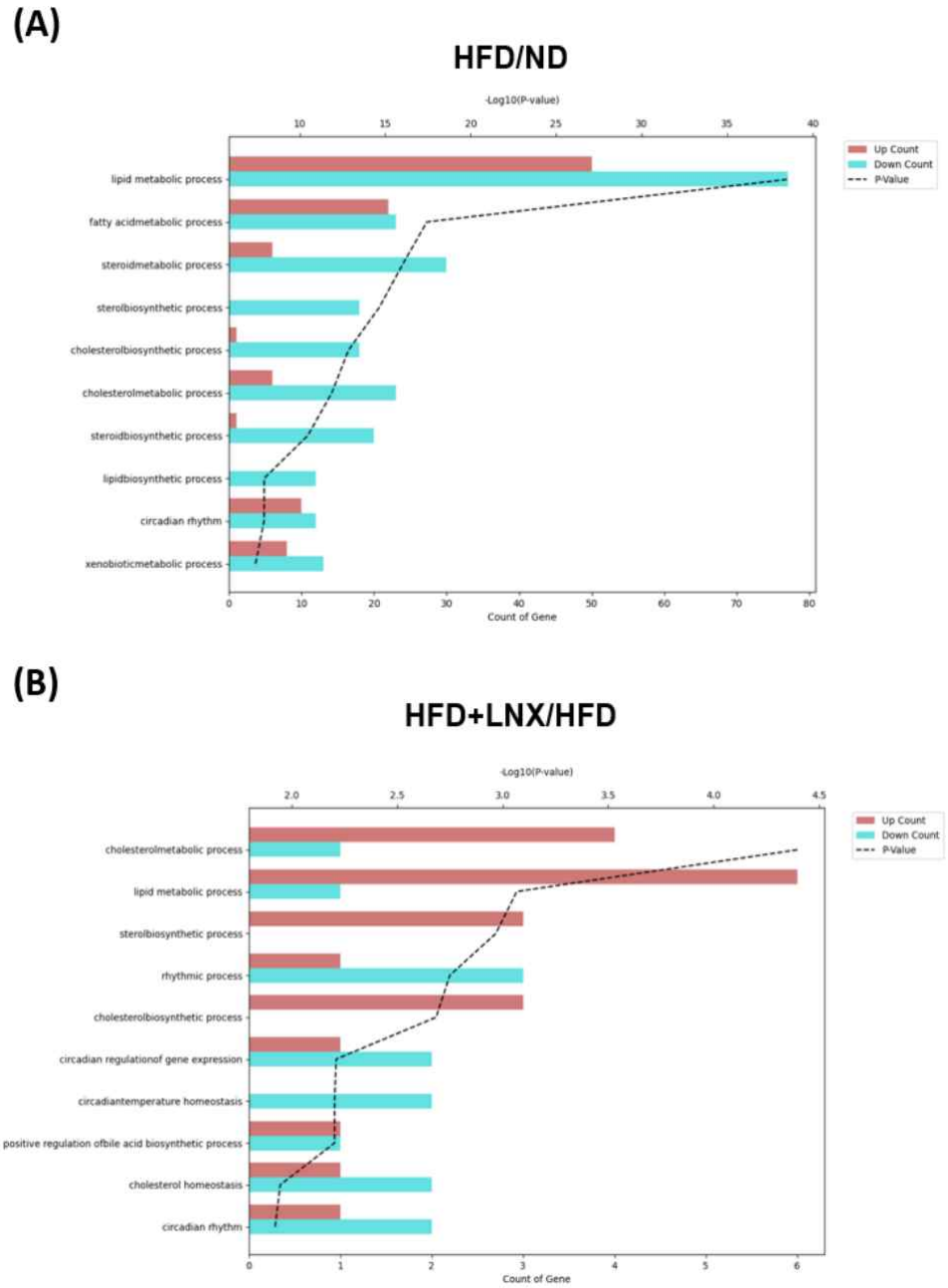

Figure 21. Probability-based GOBP analysis of mouse hepatic DEGs. DEGs in HFD compared to ND (A) and HFD-LNX compared to HFD (B) were displayed by biological category and P-value (dotted line). Red and blue bar represents up-regulated and down-regulated transcript, respectively.

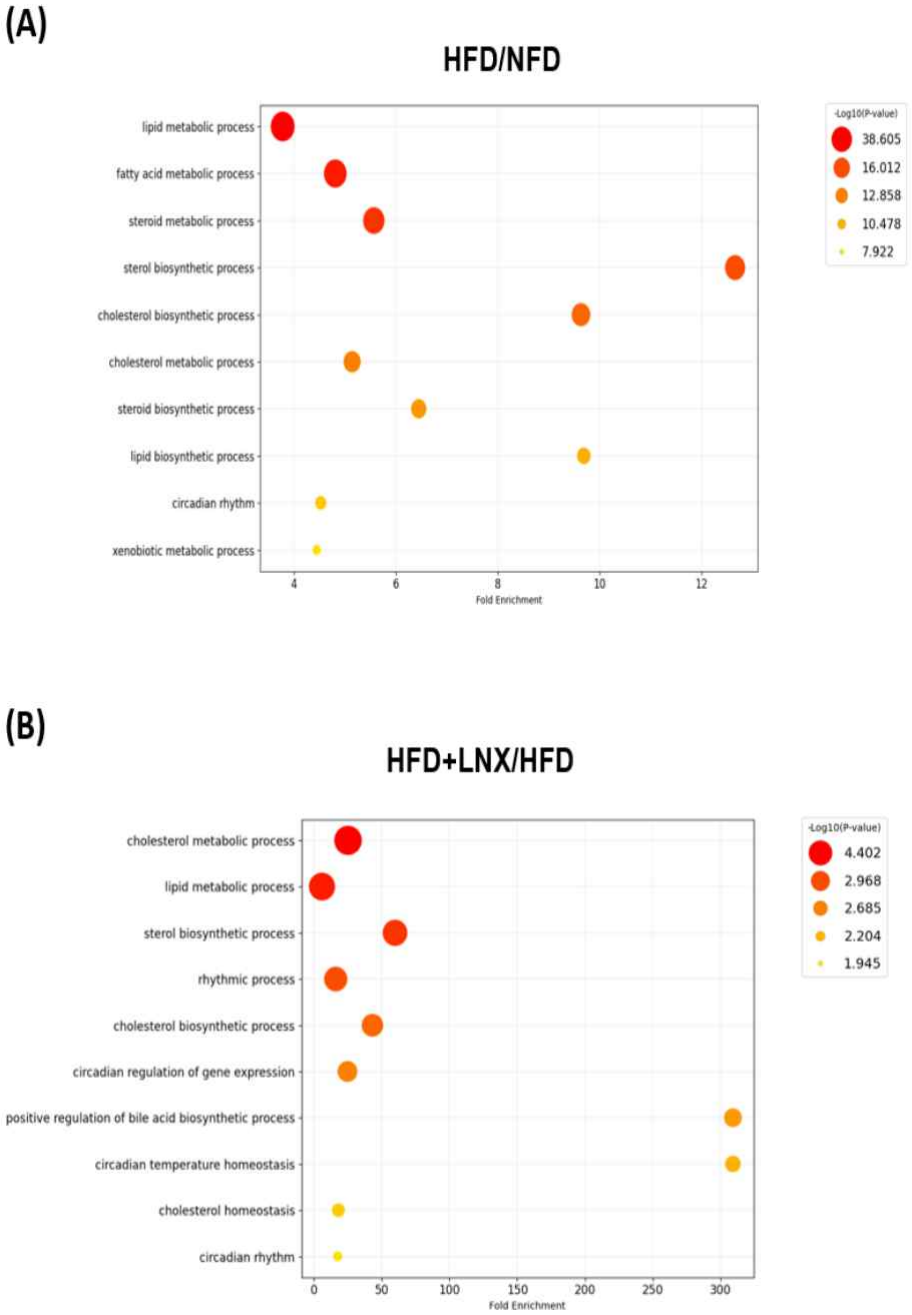

Figure 22. Fold enrichment-based GOBP analysis of mouse hepatic DEGs. DEGs in HFD compared to ND (A) and HFD-LNX compared to HFD (B) were displayed by biological category and fold enrichment. Size of round circle indicates the -log10(P-value).

9. Discovered DEGs were Mapped to KEGG Pathways

The identified differentially expressed genes (DEGs) were subjected to a detailed analysis of Kyoto Encyclopedia of Genes and Genomes (KEGG) pathways. In the comparison of high-fat diet (HFD) to normal diet (ND), major metabolic pathways such as cancer, proteasome processing, and neurodegenerative diseases were observed, with PPAR signaling ranking highest among the obesity-related pathways, involving a total of 23 genes (**Table 4**). Mapping the DEGs related to PPAR signaling revealed genes associated with receptor proteins, ligands, transcription factors, and target genes showing increased or decreased expression. The results indicated that PPAR signaling plays a prominent role in regulating target genes in obesity induced by a high-fat diet (**Figure 23**). Additionally, 19 DEGs were involved in pathways related to obesity, lipid metabolism, and atherosclerosis (**Table 4**). These genes were mapped to KEGG metabolic pathways (**Figure 24**). Increased LDL led to intracellular or ER-mediated signal transduction through cell membrane proteins RAGE, Nox1/2, and CD36, ultimately resulting in lipid drug metabolism and immune response signaling. In the comparison of LNX-HFD to HFD, key pathways included circadian rhythm, PPAR signaling, sterol metabolism, and cancer-related metabolism, each involving 2-3 mRNA transcripts (**Table 5**). Mapping the DEGs related to PPAR signaling in LNX-HFD revealed two genes, with Cyp7A1, a LNX-targeted protein related to lipid drug metabolism, showing decreased expression (**Figure 25**). In addition, Perilipin, involved in lipid droplet movement, was found to increase in expression due to LNX.

Table 4. List of DEGs mapped to KEGG pathway in HFD and ND mouse livers

Pathway Code*	Category of Biological Process	Gene Number
mmu05200	Pathway in cancer	37
mmu05207	Chemical carcinogenesis - receptor activation	29
mmu04141	Protein processing in endoplasmic reticulum	28
mmu05022	Pathway of neurodegeneration - multiple disease	28
mmu02010	Alzheimer disease	24
mmu01240	Biosynthesis of cofactors	23
mmu03320	PPAR signaling pathway	23
mmu00830	Retinol metabolism	23
mmu04145	Phagosome	22
mmu00480	Glutathione metabolism	22
mmu05418	Fluid shear stress and atherosclerosis	21
mmu04151	PI3K-Akt signaling pathway	21
mmu04015	Rap1 signaling pathway	20
mmu05204	Chemical carcinogenesis - DNA adducts	20
mmu05417	Lipid and atherosclerosis	19
mmu05225	Hepatocellular carcinoma	19
mmu05014	Amyotrophic lateral sclerosis	19
mmu00140	Steroid hormone biosynthesis	19
mmu05171	Coronavirus disease - COVID19	18
mmu00982	Drug metabolism - cytochrome P450	17
mmu04613	Neutrophil extracellular trap formation	17
mmu05020	Prion disease	17
mmu00983	Drug metabolism - other enzymes	17
mmu04936	Alcoholic liver disease	17

*mmu00000 means the biological process pathway belonged to house mouse (*Mus musculus*).

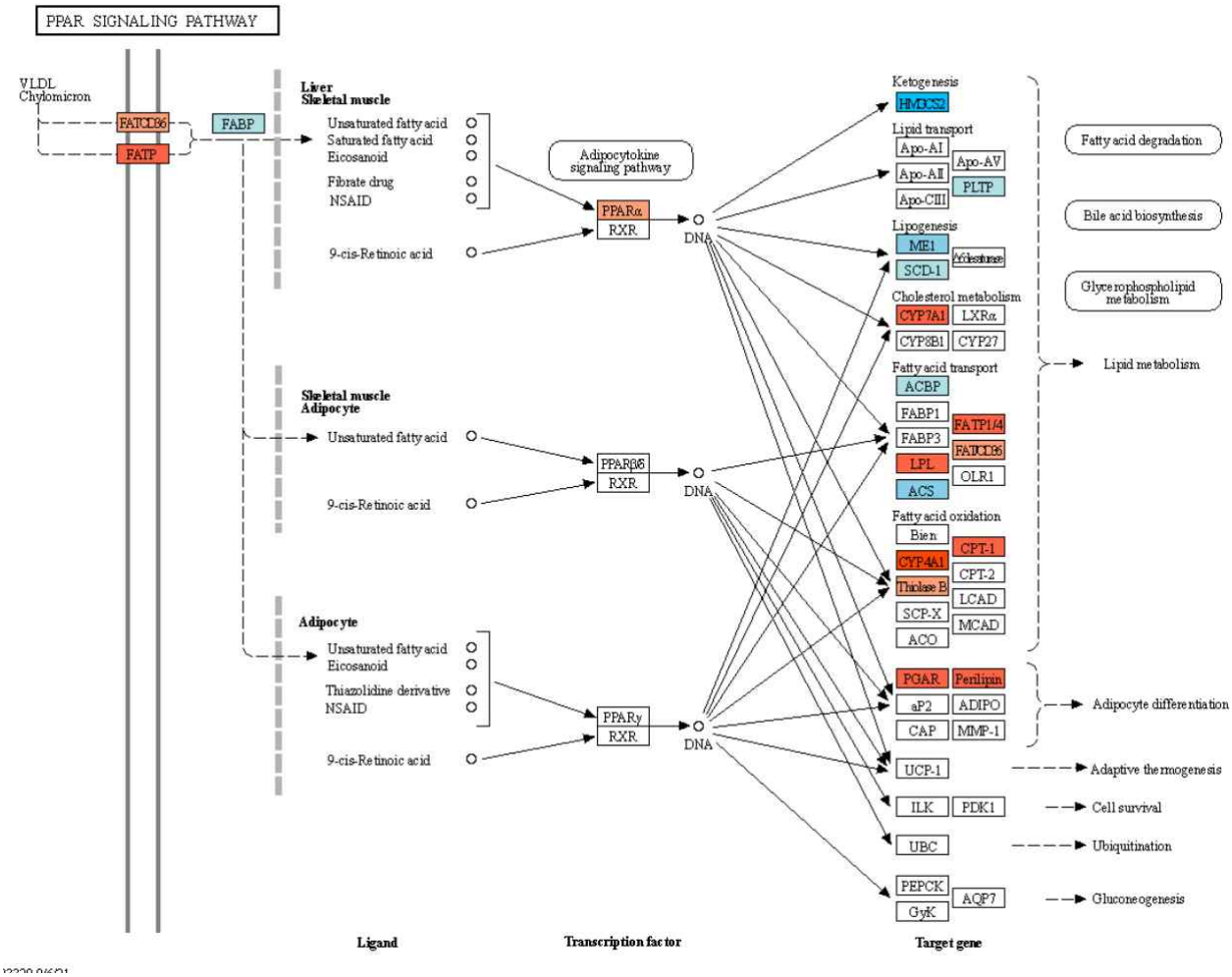

Figure 23. Mapping of DEGs in HFD and ND mouse liver to PPAR signaling pathway. Nineteen DEGs are mapped in PPAR signaling pathway. Red and blue box indicates up-regulated and down-regulated transcripts in HFD compared to ND. Images were constructed on the basis of KEGG pathway website.

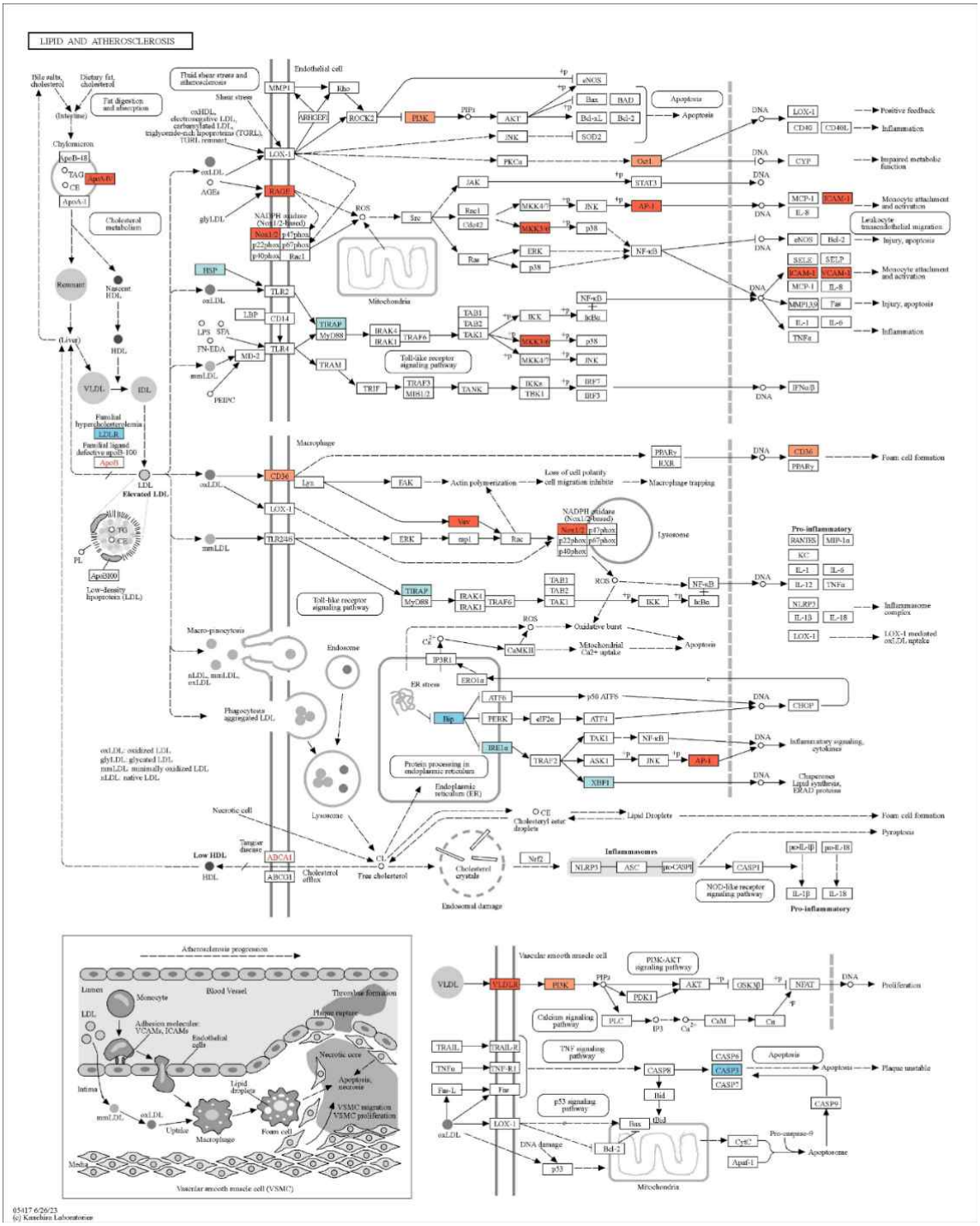

Figure 24. Mapping of DEGs in HFD and ND mouse liver to lipid and atherosclerosis pathway. Twenty-six DEGs are mapped in lipid and atherosclerosis pathway. Red and blue box indicates up-regulated and down-regulated transcripts in HFD compared to ND. Images were constructed on the basis of KEGG pathway website.

Table 5. List of DEGs mapped to KEGG pathway in LNX-HFD and HFD mouse livers

Pathway Code*	Category of Biological Process	Gene Number
mmu04710	Circadian rhythm	3
mmu03320	PPAR signaling pathway	2
mmu00100	Steroid biosynthesis	2
mmu05200	Pathway in cancer	2
mmu05202	Transcriptional mis-regulation in cancer	2
mmu05166	Human T-cell leukemia virus 1 infection	2
mmu00910	Nitrogen metabolism	1
mmu05215	Prostate cancer	1
mmu04151	PI3K-Akt signaling pathway	1
mmu00980	Metabolism of xenobiotics by cytochrome P450	1
mmu04740	Olfactory transduction	1
mmu04928	Parathyroid hormone synthesis - secretion and action	1
mmu05226	Gastric cancer	1
mmu05165	Human papillomavirus infection	1
mmu05220	Chronic myeloid leukemia	1
mmu04060	Cytokine-cytokine receptor interaction	1
mmu05205	Proteoglycans in cancer	1
mmu05164	Influenza A	1
mmu04218	Cellular senescence	1
mmu00983	Drug metabolism - other enzymes	1
mmu05225	Hepatocellular carcinoma	1
mmu04979	Cholesterol metabolism	1
mmu05206	MicroRNA in cancer	1
mmu04934	Cushing syndrome	1

*mmu00000 means the biological process pathway belonged to house mouse (*Mus musculus*).

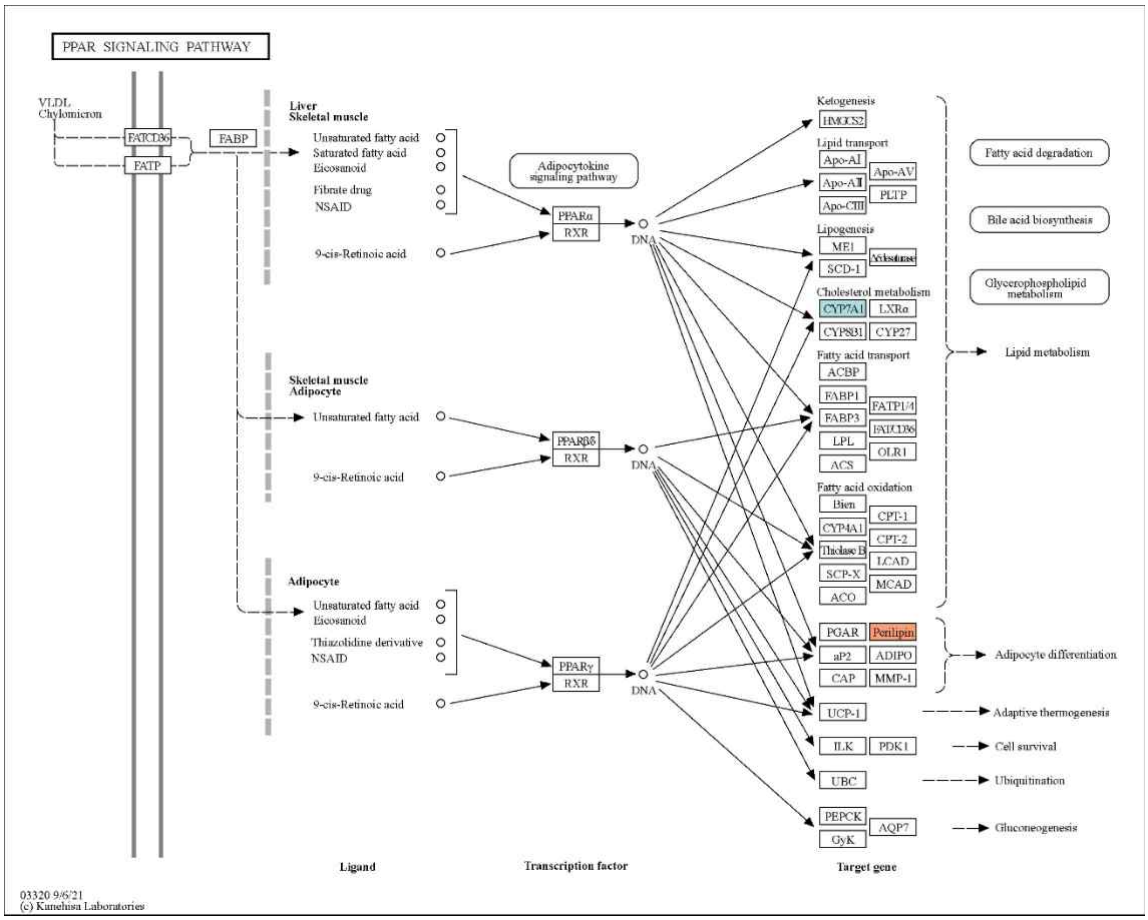

Figure 25. DEGs between LNX-HFD and HFD mouse liver in PPAR signaling pathway. Two DEGs are mapped in PPAR signaling pathway. Red and blue box indicates up-regulated and down-regulated transcripts in HFD compared to ND. Images were constructed on the basis of KEGG pathway website.

10. LNX Mainly Suppresses Immune Response and Lipid Metabolism

The comprehensive and comparative analysis of the transcriptome and proteome aimed to explore LNX-targeted genes and proteins in the context of obesity induction and anti-obesity effects. The Jaccard index and Jaccard distance were calculated based on the differential expression patterns of proteins and mRNAs. The similarity index between ND and HFD was lower compared to LNX-HFD and HFD, as indicated by Jaccard indices of 0.547 and 0.623, respectively (**Figure 26**). Weighted J-indices were 0.357 for ND/HFD and 0.392 for LNX-HFD/HFD, while J-distances were 0.453 and 0.377, respectively. Weighted J-distances were 0.643 for ND/HFD and 0.608 for LNX-HFD/HFD. Thus, both DEPs and DEGs exhibited lower similarity in ND and HFD, and LNX treatment did not significantly increase this similarity. Pearson correlation analysis of the expression levels between DEPs and DEGs showed low correlation coefficients of 0.096 for ND/HFD and 0.139 for LNX-HFD/HFD, indicating minimal correlation between proteins and transcripts (**Figure 27**).

Finally, the focus was on the common genes/proteins expressed between DEPs and DEGs. The expression patterns of 22 proteins identified in both proteome and transcriptome analyses were compared. Among the proteins commonly decreased in expression, four were identified in ND/HFD, and one was identified in LNX-HFD/HFD (**Figure 28A**). Commonly increased proteins were counted as 12 in ND/HFD and one in LNX-HFD/HFD. The 3 proteins that exhibited common changes between ND/HFD and LNX-HFD/HFD were Clec4f, S100a9, and Hsd17b6. These proteins, whose expression decreased in both immune response proteins and lipid metabolism-related proteins/mRNAs, demonstrated a consistent pattern. For the transcriptome analysis, a total of 13 significant expression-changing proteins were identified (**Figure 28B**). Among these, three proteins were common with the proteins identified in the proteome analysis: Cyp51, Thrsp, and Krt23. These proteins were related to lipid metabolism, cholesterol synthesis, and epithelial cell differentiation. Notably, the expression patterns of three proteins were opposite between LNX-treated and untreated HFD conditions. All three common proteins showed a consistent decrease at the translation level. Relative expression of selected 6 genes was presented in HFD / ND and LNX-HFD / HFD (**Figure 29**).

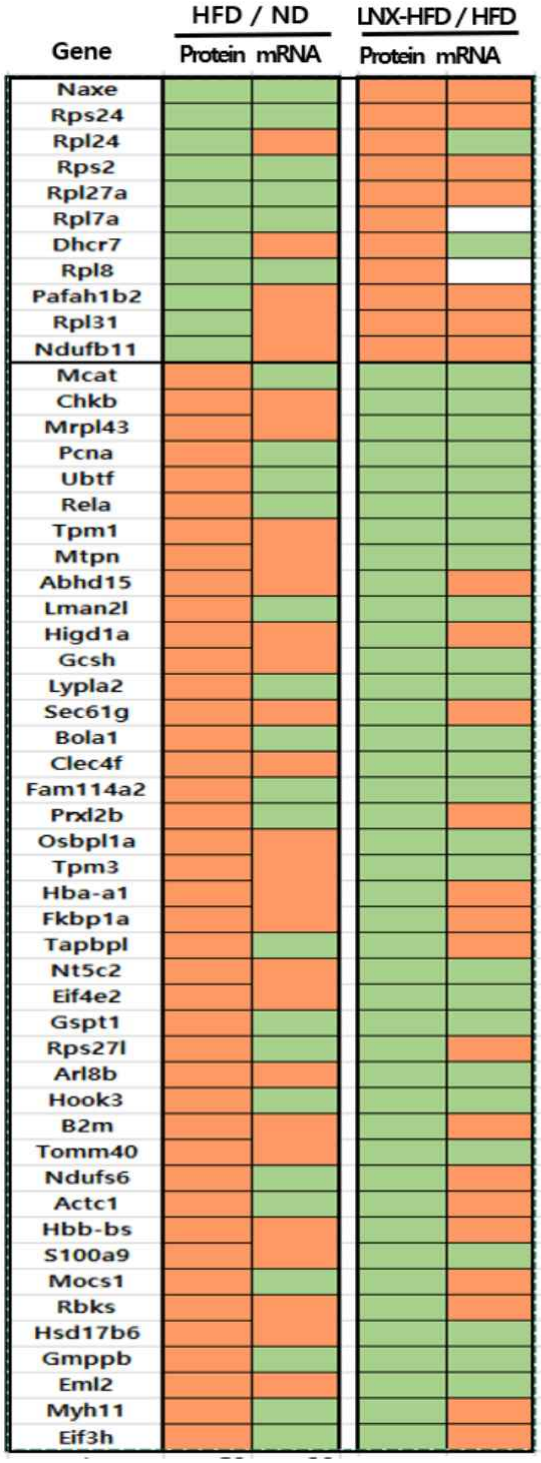

	HFD/ND	LNX-HFD/HFD
J-index	0.547	0.623
J-distance	0.453	0.377

	HFD/ND	LNX-HFD/HFD
J'-index	0.357	0.392
J'-distance	0.643	0.608

Figure 26. Similarity analysis of differentially expressed proteins and mRNA. Right box indicates the values of J and J'-index and distance. Detailed calculation was described in Materials and Methods.

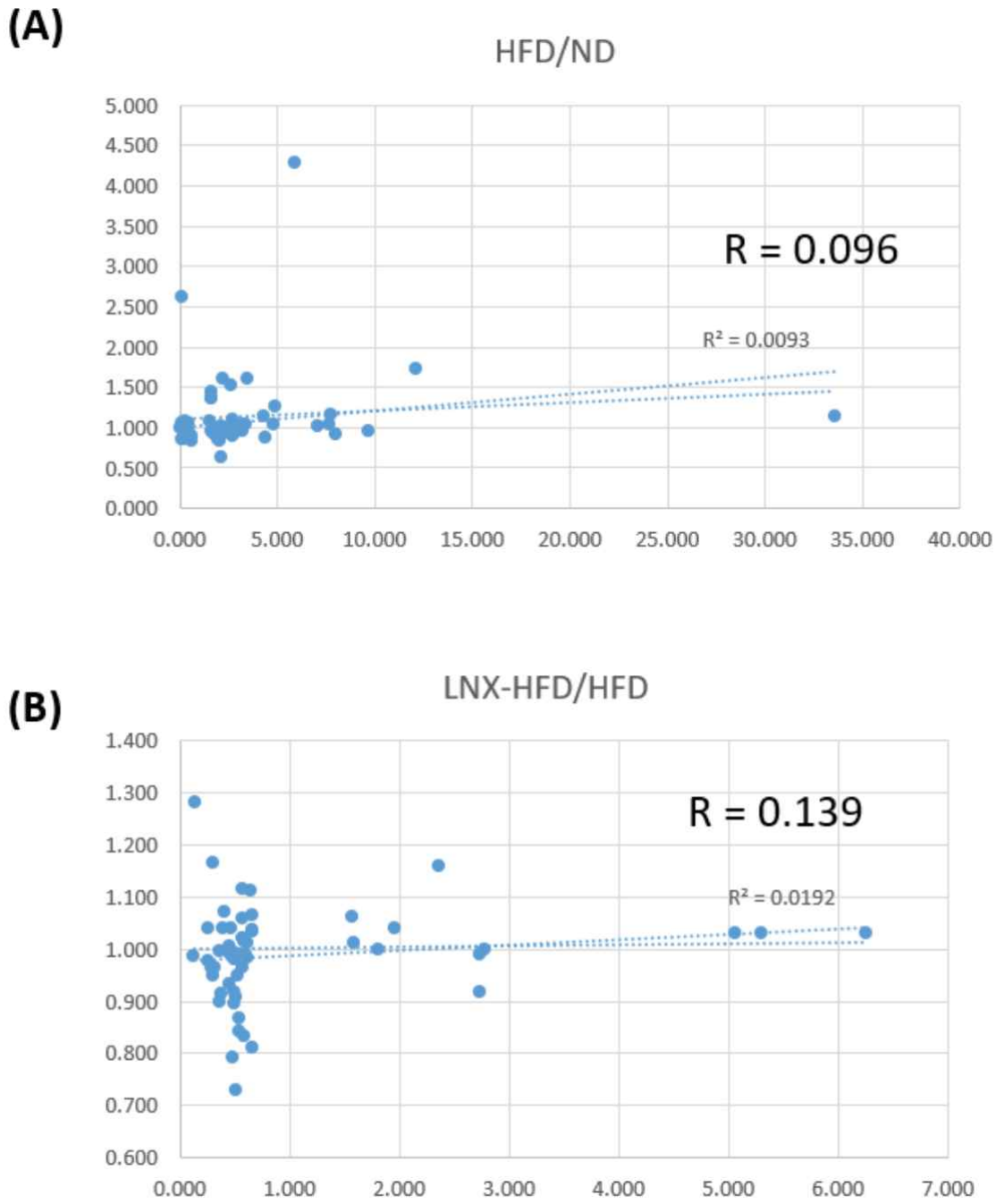

Figure 27. Correlation of differentially expressed proteins and mRNA. Selected proteins and mRNAs at P<0.05 and fold change>1.5 were fitted to linear regression curve.

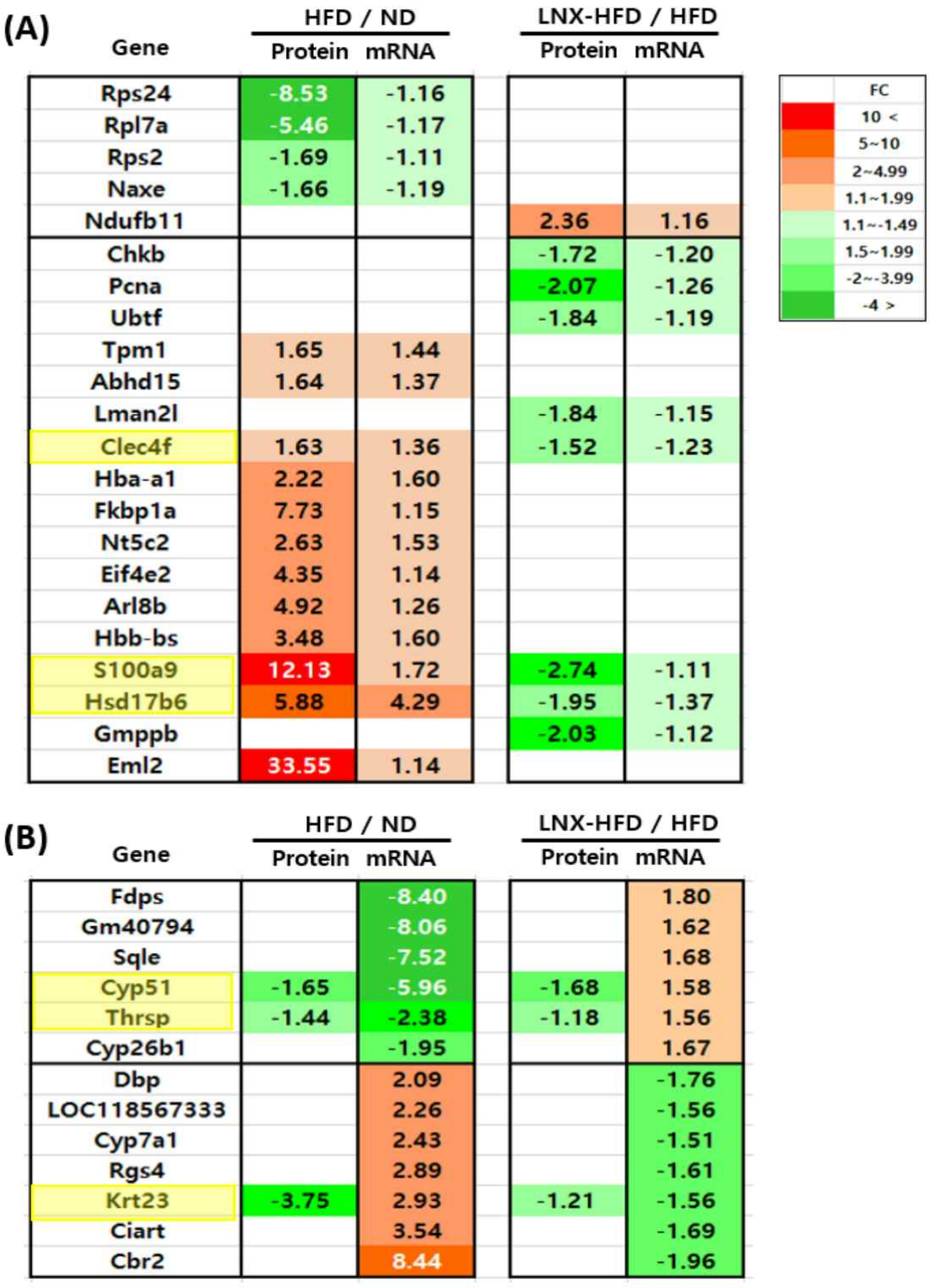

Figure 28. Comparison of commonly expressed patterns of DEGs and DEPs. Similar expression patterns of proteins (A) and mRNA (B) were presented as heat map. Six gene products (yellow highlight) were identified commonly in proteins and mRNA.

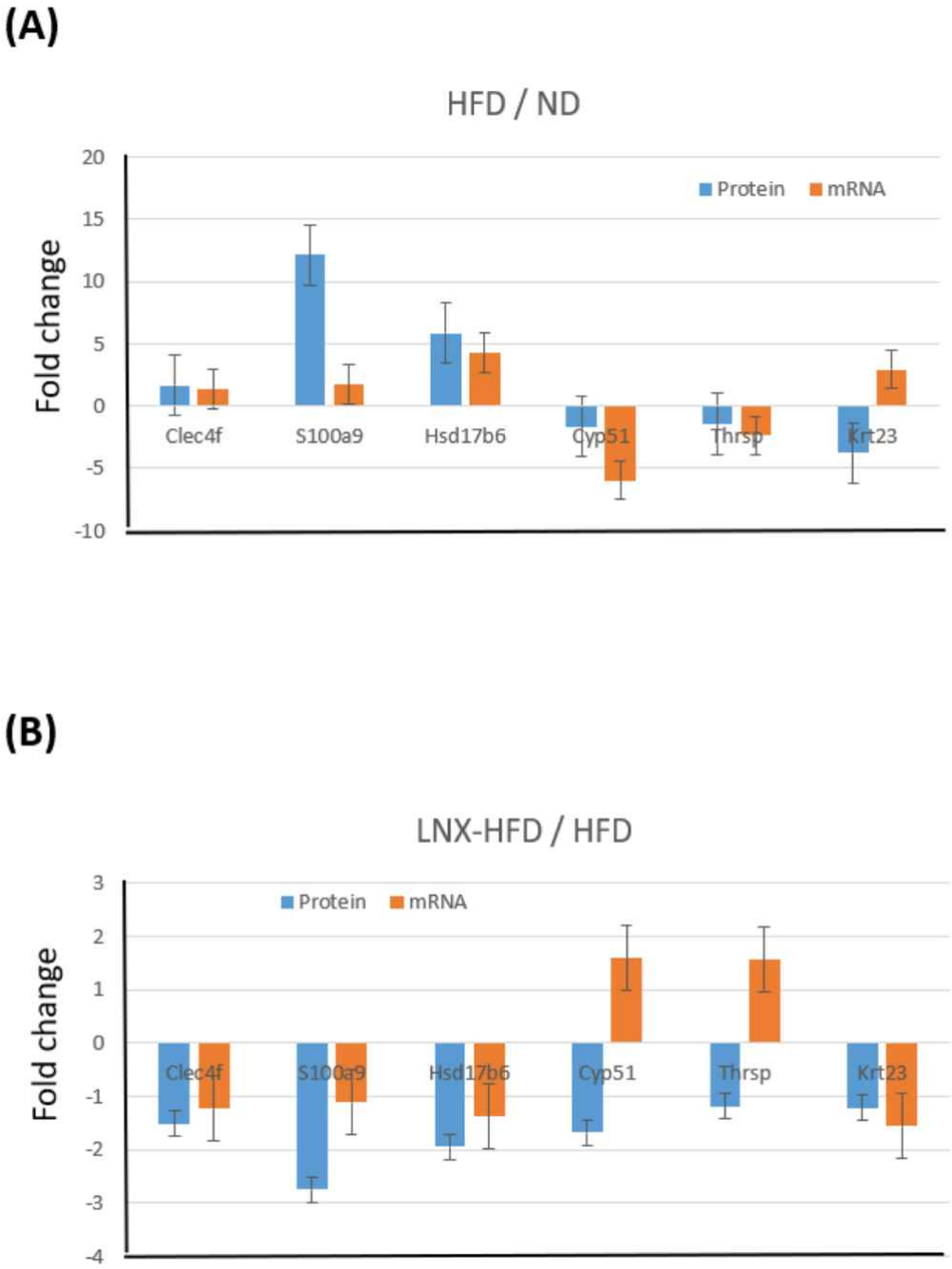

Figure 29. Relative exrpession of selected DEGs and DEPs. Selected six genes are commonly expressed in HFD / ND (A) and LNX-HFD / HFD (B). Relative fold changes were presented as average ± SD. Sample numbers : ND (n=4), HFD (n=9), LNX-HFD (n=10).

IV. Discussion

Obesity is rapidly increasing globally, posing various health issues. It is a known risk factor for chronic diseases such as diabetes, hypertension, and cardiovascular diseases, impacting not only physical health but also psychological well-being. Obesity can lead to negative psychological effects, causing depression and a decrease in self-esteem, ultimately affecting the quality of life and social interactions. Moreover, unregulated liver metabolism, resulting in hepatic obesity, is associated with obesity (Kawano and Cohen, 2013). Current obesity management includes approaches like diet, exercise, medication, and obesity surgery. Recently, there has been a tremendous demand for obesity drugs that are both stable and effective (Elangbam, 2009).

Revolutionary drugs in obesity treatment, such as Semaglutide and Tirzepatide, have released as a promising solution, inducing a 21% weight loss in clinical trials (Jastreboff et al., 2022). Semaglutide, known as Ozempic, was approved by the FDA in 2017 as a treatment for type 2 diabetes, and in 2021, it was approved for obesity treatment under the name Wegovy (Lenharo, 2023). Tirzepatide, also known as Mounjaro, received approval for diabetes treatment in 2022 and has been prescribed for weight loss purposes as well. However, a study on obese patients revealed a 4.6 times higher incidence of pancreatitis in those taking Semaglutide compared to those taking weight loss drugs that mimic GLP-1 (Sodhi et al., 2023). Therefore, despite the remarkable efficacy of pharmacological treatments, the issue of underlying side effects persists.

An alternative to the synthetic chemical drug has emerged in the form of natural anti-obesity agents. Natural substances modify the host's metabolism processes, stimulate metabolism and heat generation, regulate appetite, inhibit pancreatic lipase and amylase enzymes, increase insulin sensitivity, inhibit fat formation, and induce apoptosis of fat cells to maintain glucose homeostasis (Sayed et al., 2023). Some phytochemicals have shown potential in reducing inflammatory substances such as TNF-α, IL-6, and IL-1 secreted from adipose tissue, thereby regulating weight through changes in leptin and adipokine production. Natural substances are categorized into single compounds, foods, fruits, and herbal medicines (single extracts,

decoctions). These medicinal materials are typically explained through mechanisms such as anti-obesity, anti-inflammatory, antioxidant, appetite suppression, and heat generation. Natural anti-obesity agents, mainly studied ingredients, include coffee, green tea, garlic, Gambisan, and Euiiying-tang (Park et al., 2023). Natural anti-obesity agents are gaining attention as an innovative approach to obesity management, focusing on minimizing side effects and maximizing effectiveness by utilizing components extracted from natural sources, such as plants or seaweed.

In this study, a natural extract of nutmeg (LNX) was utilized as an anti-obesity agent. Nutmeg extract is known to affect gut health, containing various lignan compounds that alter gut microbiota, regulate NASH, inhibit intrahepatic fat accumulation, and enhance liver function (Yang et al., 2022). Recent mechanistic studies have been conducted on the anti-obesity effects of nutmeg extract (Perumal et al., 2024). Nutmeg, originating from the Maluku Islands in Indonesia, has long been used as a spice ingredient. Nutmeg seeds and mace have been reported to have various health benefits, including anti-obesity, anti-diabetic, antimicrobial, antioxidant, and anti-inflammatory properties (Nguyen et al., 2010; Zhao et al., 2022; Lesmana et al., 2021). However, nutmeg seeds contain alkylbenzene derivatives such as myristicin, elemicin, and safrole, which can induce hallucinogenic symptoms (Götz et al., 2022). Therefore, a technology has been developed to remove toxic substances and concentrate the representative compound nectandrin B of the effective component lignan, confirming its muscle atrophy improvement effect (Lee et al., 2023).

The enhanced lignan nutmeg extract (LNX) used in this study contains less than 0.5% toxic myristicin and is enriched with nectandrin B. Actual analysis of nectandrin B content revealed 82%, as shown in **Figure 2**. When LNX was treated on pre-adipocytes 3T3-L1, it reduced STAT3 phosphorylation but had a limited impact on the expression of PPAR-γ and C/EBP-α. Instead, it decreased fatty acid synthase (FAS) without stimulating glycerol secretion and hormone-sensitive lipase phosphorylation. In conclusion, it was demonstrated that LNX has an anti-obesity effect by inhibiting STAT3 phosphorylation and FAS expression. However, the study does not explain the genomic-level changes in the entire transcriptome (mRNA, protein) regarding the anti-obesity effects of LNX at the actual in vivo level.

Obesity research investigates pathological phenomena in specific genetic backgrounds through experiments targeting obesity-related genes. A representative example is the use of genetically modified mice, such as *ob/ob* mice with leptin gene knockout, to induce obesity and study genetic models. During the progression of obesity in *ob/ob* mice, an increase in peroxisome proliferator-activated receptor (PPAR) and protein secretion in the liver was observed. Protein analysis revealed alterations in lipid and cholesterol metabolism, protein interactions, and regulation of immune system-related proteins (Stocks et al., 2022). Obesity also leads to distinctive increases in proteins related to liver lipid metabolism. Excessive appetite and energy intake contribute to the manifestation of obesity and hepatic steatosis in obese mice (Jequier, 2002). However, disruptions in obesity-related genes may result in differences from the natural obesity process due to disturbances in other genetic networks and alternative gene reconfigurations. Natural obesity involves transforming the phenotype through diet-induced obesity. For instance, Smith et al. (2021) administered a high-fat diet, a known inducer of obesity, to mice for 8 weeks, investigating weight gain, insulin resistance, and changes in adipose tissue. Such dietary mouse models contribute to understanding the physiological changes associated with obesity induced by high-fat diets. Obesity induced by a high-fat diet gradually progresses to NASH (Boland et al., 2019). The pathology of NASH is characterized by inflammatory reactions and fibrosis associated with fat accumulation in the liver. Quantitative histological studies reveal changes at the mRNA and protein levels, including lipid accumulation, inflammation, and collagen protein deposition in liver tissues.

This experiment involved *ad libitum* feeding of a diet and water for six months, with the addition of LNX to the diet to achieve final concentrations of 0.01% and 0.1%. As observed in **Figure 3**, weight gain significantly decreased by 24% ($P<0.001$) and 17% ($P<0.05$) in the low and high LNX intake groups compared to HFD over the six months. Additionally, as shown in **Figure 5**, LNX reduced blood glucose, neutral fat, and total cholesterol. This effect is comparable to the weight loss and lipid-lowering effects of berberine (Ilyas et al., 2020). Furthermore, besides a high-fat diet (HFD), reports indicate that high-fat and high-cholesterol diets result in higher levels of various biochemical markers (Liang et al., 2021). Similarly, the natural substance glycyrrhizic acid lowers blood glucose, enhances insulin sensitivity, and alters lipid metabolism profiles. Specifically, the enzyme 11β-hydroxysteroid dehydrogenase, involved in lipid metabolism, was reduced in the liver (Ton et al., 2013). One of the most

surprising aspects of LNX's anti-obesity effect is the significant reduction in body fat content and the decrease in fat accumulation rate and size of fat cells in the liver and adipose tissue, as depicted in **Figures 7** and **9**. Analysis of body fat composition using DEXA in HFD, as conducted in a previous study with Balb/C mice fed a high-fat diet rich in fatty acids, confirmed these findings (Arunabh et al., 2005).

One notable finding is that HFD increases bone density, while LNX decreases it, as shown in **Figure 8**. However, previous reports had suggested that high-fat diets weaken bone formation (Qiao et al., 2021). This discrepancy might be attributed to differences in mouse strains and rearing environments. BMD by LNX decreased, but BMC increased, suggesting some qualitative improvement in bone despite the reduction in bone mineral density. According to previous reports, BMC is higher in low-fat diets compared to high-fat diets (Wohl et al., 1998), indicating that further research on bone components based on dietary conditions needs to be conducted. In obesity research, mouse models are crucial tools for understanding the physiological and molecular characteristics related to human obesity. Recent studies have reported cases of omics research related to obesity using mice. Metabolic analysis of the liver TCA circuit in high-fat diet mouse models reported an increase in malate, succinate, and oxaloacetate (Sundekilde et al., 2020). Additionally, multi-omics reports on obesity-related immune cell phenotypes in mouse adipose tissue during weight loss and gain have been documented (Cottam et al., 2022). Moreover, analyzing liver and plasma proteins from obese mouse models has been performed to study tissue interplay (Stock et al., 2022).

This study compared protein expression at the genome-wide level by extracting proteins from mouse liver tissues under conditions of natural obesity induced by a high-fat diet and an HFD with added LNX. Approximately 2000 proteins were identified for each condition (**Table 2**, **Figure 10**). The variability of individual proteins in the ND, HFD, and LNX-HFD groups narrowed to a range of 0~20% (**Figure 11**), and clear group distinctions were observed in individual clustering heat map analysis (**Figure 12**). The comparative protein analysis results, summarized in **Table 3**, showed that translation proteins decreased under HFD conditions but were restored by LNX. This suggests that LNX may restore the decreased protein translation ability under obesity conditions (**Figure 15**). Similar reports indicated a decrease in mitochondrial translation under obesity conditions (Perks et al., 2020). As predicted, the number

of genes related to lipid metabolism changed in the HFD condition and was reversed by LNX. It was notable that peroxisome proliferation, a representative aspect of liver lipid metabolism, was regulated (Fujiki et al., 2014). Notably, proteins related to metabolic processes, mitochondrial function, and immune response that increased in HFD were restored by LNX. High-fat diets are known to impair the regulatory ability of immune cells (Kiran et al., 2022), so the alteration of immune action by LNX is highly significant.

This time, a comparative analysis of the transcriptome in liver tissues under ND, HFD, and LNX-HFD conditions was conducted. Through cluster heat map analysis, 13 differentially expressed genes (DEGs) were observed (**Figure 18**). Genes whose expression increased by LNX were related to cholesterol synthesis, such as Cyp51 and Fdps. Conversely, genes whose expression decreased by LNX were associated with circadian rhythm, hormone synthesis processes, and epithelial cell differentiation. In mouse liver tissues under high-fat diet conditions compared to normal diet, the PPAR signaling pathway, a central pathway in lipid metabolism through the PPAR signaling pathway, was disturbed, with Cyp7A1 at the center. Changes in Cyp7a1 under high-fat diet conditions have been reported previously (Duan et al., 2019). Among the genes altered by LNX under HFD conditions, the cholesterol metabolism-related Cyp7a1 decreased, and the key protein for lipid mobilization, perilipin, increased (**Figure 25**). The opposite expression regulation of Cholesterol 7α-hydroxylase (Cyp7a1) and perilipin has been similarly observed in previous studies (Enjoji et al., 2016).

In this study, the comparison of transcriptomes and proteomes accumulated independently from the same mouse liver tissues revealed that only four out of 13 DEGs identified from the transcriptome were connected to DEPs. However, the expression patterns were significantly different between the transcriptome and proteome. The mismatch between transcriptome and proteome expression in eukaryotes is consistent with previous findings (Ghazalpour et al., 2011). This mismatch arises due to the complexity of pre-translational and post-translational processes such as protein degradation, translation efficiency, and movement to intracellular organelles, in the context of the translation after transcription until the functional protein is expressed (Lundberg et al., 2010). Jaccard dissimilarity analysis confirmed that the correlation between ND and HFD was lower than that between HFD and LNX-HFD (**Figure 26**). As the dietary conditions differed, they could be adequately explained, and LNX feeding did not cause significant differential gene changes compared to HFD alone. When examining the correlation

between differentially expressed genes (DEGs) and differentially expressed proteins (DEPs) using Pearson correlation analysis, the correlation was very low (**Figure 27**), consistent with previous reports (Krahmer et al., 2018). When comprehensively analyzing the expression patterns of DEGs and DEPs, unique to the transcriptome and proteome in mouse liver tissues under high-fat diet conditions and high-fat diet conditions with LNX, a total of six genes were identified and relative expression% of DEPs and DEGs was presented (**Figure 28, 29**).

The genes and proteins related to lipid metabolism include Thrsp, Hsd17b6, cholesterol synthesis-related Cyp51, immune response-related Clec4f, S100a9, and epithelial cell differentiation-related Krt23 were identified. Clec4f, known to be identified by C-type lectins in Kupffer cells in mice (Scott et al., 2016), induces neutral fat accumulation during the progression of NASH (Tran et al., 2020). However, the decrease in Clec4f expression by LNX, while it increased in high-fat diet (HFD), is explained as the cause of the reduction in neutral fat content. S100a9, when overexpressed in obesity, hinders Kupffer cell differentiation in the TLR4-NFkB signaling pathway, making inflammation and wound healing difficult (Franz et al., 2022). LNX-induced suppression of S100A9 expression is presumed to play a crucial role in the anti-obesity mechanism. Hsd17b6 is known to delay the onset of type 2 diabetes by inhibiting the activity of the transcription factor SREBP (Wei et al., 2023). HSD17B6 delays the development of obesity-induced type 2 diabetes and enhances resistance to glucose. However, excessive expression of Hsd17b6 in a high-fat diet may, in turn, induce complications derived from obesity. Therefore, inhibition by LNX is estimated to induce a return to normal metabolic processes.

In summary, the comprehensive results suggest that the anti-obesity effects of LNX, such as weight loss, significant reduction in visceral fat, and decreases in blood glucose and LDL, are manifested at the gene/protein level by inhibiting lipid metabolism, cholesterol synthesis, immune response, and epithelial cell differentiation processes (**Figure 30**). Current medical basic research trends are expanding into the study of interactions between complex diseases caused by obesity. Starting with clues indicating that high-fat diets induce chronic inflammation (Rohm et al., 2022), further comprehensive studies are needed to identify genetic/protein targets related to obesity, inflammation, immune response, and lipid metabolism affected by LNX.

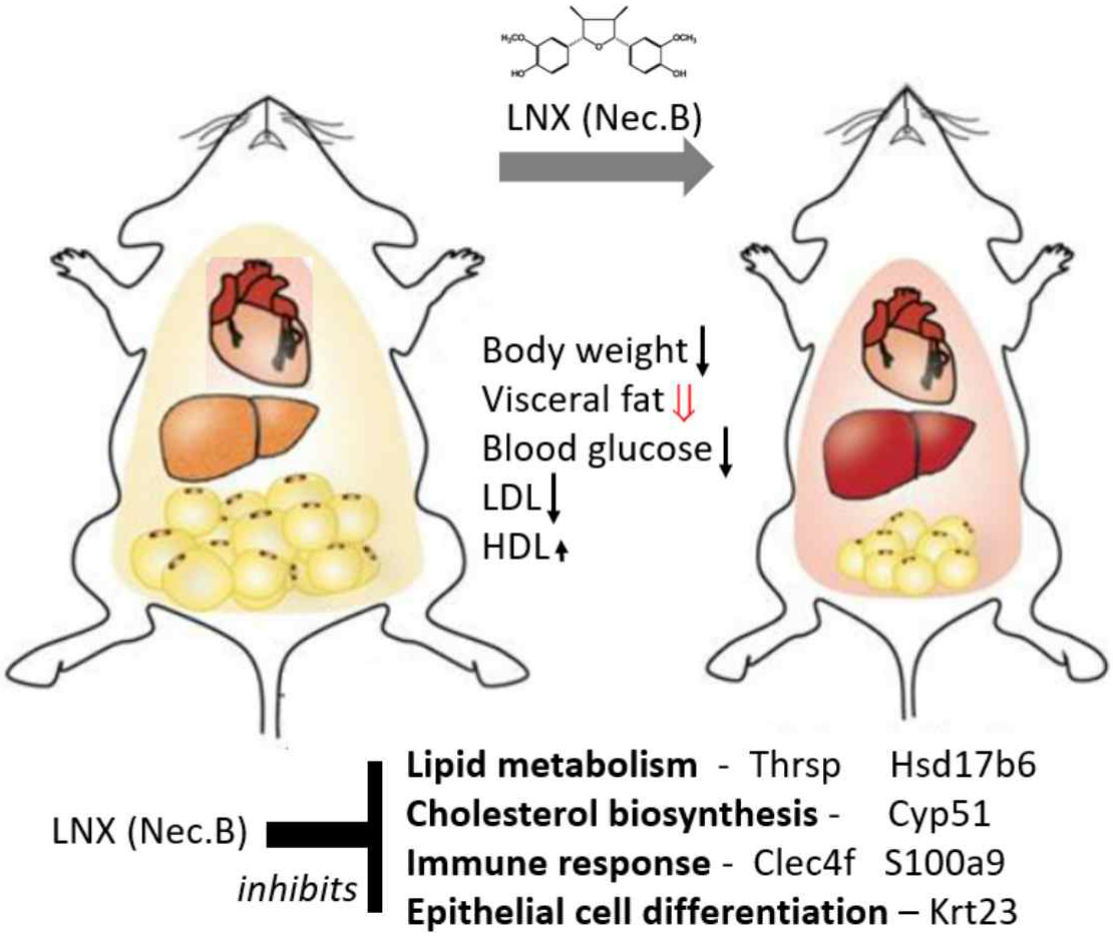

Figure 30. Hypothetical working model of anti-obesity action of LNX in mouse. Proposal of LNX inhibition to six gene products was based on the protein expression level in LNX-HFD/HFD.

V. Conclusion

The main objective of this study was to explore anti-obesity-related proteins in mice induced with obesity through *ad libitum* feeding of LNX under a high-fat diet condition. In a long-term animal experiment, LNX containing 82% nectandrin B improved physiological obesity-related factors, and six related genes/proteins were identified.

1. Under HFD conditions, an increase in body weight, blood glucose, neutral fat, and total cholesterol was observed at 3 and 6 months, along with a significant increase in body fat content as analyzed by body composition.

2. When LNX was ingested along with HFD, there was a significant reduction in weight gain, and body fat content dramatically decreased.

3. While bone density increased under HFD conditions, some side effects were observed with a decrease in bone mineral density (BMD) due to LNX. However, bone area increased, and other bone-related indices showed no significant changes.

4. Analysis of the whole transcriptome of liver tissues from ND, HFD, and LNX-HFD mice resulted in the identification of 13 target genes, and protein analysis revealed 22 targets.

5. There was almost no correlation between the expression patterns and profiles of the transcriptome and proteome in mouse liver tissues.

6. Through systematic omics analysis, six commonly expressed proteins (Thrsp, Hsd17b6, Cyp51, Clec4f, S100a9, Krt23) were confirmed to be inhibited by LNX.

In conclusion, LNX demonstrated an effect of improving most anti-obesity indices in mice induced with obesity. LNX exhibited anti-obesity effects by inhibiting genes related to lipid metabolism, cholesterol synthesis, immune response, and epithelial cell differentiation.

References

Aegidius HM, Veidal SS, Feigh M, Hallenborg P, et al., (2020) Multi-omics characterization of a diet-induced obese model of non-alcoholic steatohepatitis. *Sci Rep* 10, 1148.

Afshin A, Forouzanfar MH, Reitsma MB, Sur P, et al., (2015) Health effects of overweight and obesity in 195 countries over 25 years. *New England J Med* 377, 13-27.

Ahn JS, Mahbub NS, Kim S, Kim HB, et al., (2023) Nectandrin B significantly increases the lifespan of Drosophila (Nectandrin B for longevity). *Aging* in printing.

Al-Hussaniy HA, Alburghaif AH, Naji MA, (2021) Leptin hormone and its effectiveness in reproduction, metabolism, immunity, diabetes, hopes and ambitions. *J Med Life* 14, 600-605.

Anders S, Pyl PT, Huber W, (2015) HTSeq-a Python framework to work with high-throughput sequencing data. *Bioinformatics* 31, 166-169.

Anstee QM, Goldin RD, (2006) Mouse models in non-alcoholic fatty liver disease and steatohepatitis research. *Int J Exp Pathol* 87, 1-16.

A**runabh B, Mizanur R, Dongxu S, Richard L, et al.,** (2005) The combination of dietary conjugated linoleic acid and treadmill exercise lowers gain in body fat mass and enhances lean body mass in high-fat–fed male Balb/C mice. *J Nutr* 135, 1124-1130.

Boland ML, Oro D, Tølbøl KS, Thrane ST, et al., (2019) Towards a standard diet-induced and biopsy-confirmed mouse model of non-alcoholic steatohepatitis: Impact of dietary fat source. *World J Gastroenterol* 25, 4904-4920.

Chung NC, Miasojedow B, Startek M, Gambin A, (2019) Jaccard/Tanimoto similarity test and estimation methods for biological presence-absence data. *BMC Bioinformatics*. 20 (Suppl 15), 644.

Cohen JC, Horton JD, Hobbs HH, (2011) Human fatty liver disease: Old questions and new insights. *Science* 332, 1519-1523.

Colquitt JL, Pickett K, Loverman E, Frampton E, (2014) Surgery for weight loss in adults. *Cochrane Database of System Rev* 2014, CD003641.

Cottam MA, Caslin HL, Winn NC, Hasty AH. (2022) Multi-omics reveals persistence of obesity-associated immune cell phenotypes in adipose tissue during weight loss and weight regain in mice. *Nature Comm* 13, 2950.

Cox J, M Mann, (2012) 1D and 2D annotation enrichment: A statistical method integrating quantitative proteomics with complementary high-throughput data. *BMC Bioinformatics* 113, S12.

Cushny AR, (1908) Nutmeg poisoning. *Proc R Soc Med* 1, 39-44.

Dobin A, Davis CA, Schlesinger F, Drenknow J, et al., (2013) STAR: ultrafast universal RNA-seq aligner. *Bioinfomatics* 29, 15-21.

Duan Y, Zhang F, Yuan W, Wei Y, et al., (2019) Hepatic cholesterol accumulation ascribed to the activation of ileum Fxr-Fgf15 pathway inhibiting hepatic Cyp7a1 in high-fat diet-induced obesity rats. *Life Sci.* 232, 116638.

Egami R, Kokaji T, Hatano A, Yugi K, et al., (2021) Trans-omics analysis reveals obesity-associated dysregulation of inter-organ metabolic cycles between the liver and skeletal muscle. *iScience* 24, 102217.

Ehrenpreis, JE, Deslauriers C, Lank P, Armstrong PK, et al., (2014) Nutmeg poisonings; A retrospective review of 10 years' experience from the Illinois poison center, 2001-2011. *J Med Toxicol* 10, 148-151.

Elangbam CS, (2009) Review paper: Current strategies in the development of anti-obesity drugs and their safety concerns. *Vet Pathol* 46, 10-24.

Enjoji M, Kohjima M, Nakamura M. (2016) Lipid metabolism and the liver. *In* Liver Systemic Diseases. pp 105-222, Springer.

Fiedman JM, Halaas JL, (1998) Leptin and the regulation of body weight in mammals. *Nature* 395, 763-770.

Franz S, Ertel A, Engel KM, Simon JC, et al., (2022) Overexpression of S100A9 in obesity impairs macrophage differentiation via TLR4-NFkB-signaling worsening inflammation and wound healing. *Theranos* 12, 1659-1682

Fujiki Y, Okumoto K, Mukai S, Honsho M, et al., (2014) Peroxisome biogenesis in mammalian cells. *Front Physiol* 5, 307.

Gentleman R, Carey WV, Bates DM, Bolstad B, et al., (2004) Bioconductor: open software

development for computational biology and bioinformatics. *Genome Biol* 5, R80.

Ghanemi A, Yoshihoka M, St-Amand J, (2018) Broken energy homeostasis and obesity pathogenesis: The surrounding concepts. *J Clin Med* 7, 453.

Ghazalpour A, Bennett B, Petyuk VA, Orozco L, et al., (2011) Comparative Analysis of Proteome and Transcriptome Variation in Mouse. *PloS Genet* 7, e1001393.

Götz ME, Sachse B, Schäfer B, Eisenreich A (2022) Myristicin and elemicin: Potentially toxicalkenylbenzenes in food. *Foods* 11, 1988.

Hack CJ, (2004) Integrated transcriptome and proteome data: the challenges ahead. *Brief Funct Genom Proteom* 3, 212-219.

Haslam DW, James WP, (2005) Obesity. *Lancet* 366, 1197-1209.

Hebebrand J, Hildebrandt T, Schlöl H, Seitz J, et al., (2022) The role of hypoleptinemia in the psychological and behavioral adaptation to starvationL Implications for anoxeia nervosa. *Neurosci Biobehav Rev* 141, 104807.

Hien TT, Oh WK, Nguyen PH, Oh SJ, et al., (2011) Nectandrin B activates endothelial nitric oxide synthase phosphorylation in endothelial cells:Role of the AMP-activated protein kinase/estrogen receptor α/phosphatidylinositol 3-kinase/Akt pathway. *Mol Pharmacol* 80, 1166-1178.

Hong J, Gu H, Lee J, Lee W, et al., (2023) Intuitive Modification of the Friedewald Formula for Calculation of LDL-Cholesterol. *Ann Lab Med* 43, 29-37.

Ilyas Z, Perna S, Al-thawadi S, Alalwan TA, et al., (2020) The effect of Berberine on weight loss in order to prevent obesity: A systematic review. *Biomedicine Pharmather* 127, 110137.

Jastreboff AM, Aronne LJ, Ahmad NN, Wharton S, et al., (2022) Tirzepatide once weekly for the treatment of obesity. *N Engl J Med* 387, 205-216.

Jang, HJ, Yang KE, Oh WK, Lee SI, et al., (2019) Nectandrin B-mediated activation of the AMPK pathway prevents cellular senescence in human diploid fibroblasts by reducing intracellular ROS levels. *Aging* 11, 3731–3749.

Jastreboff AM, Aronne LJ, Ahmad NN, Wharton S, et al., (2022) Tirzepatide once weekly for the

treatment of obesity. *New Engl J Med* 387, 205-216.

Jensen MD, Ryan DH, Apovian CM, Ard JD, et al., (2014) 2013 AHA/ACC/TOC guideline for the management of overweight and obesity in adults: a report of the American College of Cardiology/American Heart Association Task Force on Practice Guidelines and The Obesity Society. *Circulation* 129 Suppl 2, S102-S138.

Jequier E, (2002) Leptin signaling, adiposity, and energy balance. *Ann NY Acad Sci* 967, 379-388.

Kawano Y, Cohen, DE, (2013) Mechanisms of hepatic triglyceride accumulation in non-alcoholic fatty liver. *J Gastroenterol* 48, 434-441.

Kiran S, Rakin A, Kodidela S, Kumar S, et al., (2022) High-fat diet-induced dysregulation of immune cells correlates with macrophage phenotypes and chronic inflammation in adipose tissue. *Cells* 11, 1327.

Kirpich IA, Gobejishvili LN, Homme MB, Waigel S, et al., (2011) Integrated heaptic transcriptome and proteome analysis of mice with high-fat diest-induced nonalcoholoc fatty liver disease. *J Nutr Biochem* 22, 38-45.

Kojima M, Hosoda H, Date Y, Nakazato M, et al., (1999) Ghrelin is a growth-hormone-releasing acylated peptide from stomach. *Nature* 402, 656-660.

Krahmer N, Najafi B, Schueder F, Quagliarini F, et al., (2018) Organellar proteomics and phospho-proteomics reveal subcellular reorganization in diet-induced hepatic steatosis. *Dev Cell* 47, 205-221.e7.

Lape P, Peterson E, Tanudirjo D, Shiung CC, et al., (2018) New data from an open neolithic site in eastern Indonesia. *Asian Persp* 57, 222-243.

Lee JH, Kang H, Ban KT, Kim BK, et al., (2023) Proteome network analysis of skeletal muscle in lignan-enriched nutmeg extract fed mice. *J Anal Sci Tech* 14, 11.

Lenharo M, (2023) Anti-obesity drugs' side effects: what we know so far. *Nature* 622, 682.

Lesmana R, Siannoto M, Nugraha GI, Goenawan H, et al., (2021) Nutmeg extract potentially alters characteristics of white adipose tissue in rats. *Vet Med Sci* 7, 512-520

Liang H, Jiang F, Cheng R, Luo Y, et al., (2021) A high-fat diet and high-fat and high-cholesterol diet may affect glucose and lipid metabolism differentially through gut microbiota in mice. *Exp Anim* 70, 73-83.

Lundberg E, Fagerberg L, Klevebring D, Matic I, et al., (2010) Defining the transcriptome and proteome in three functionally different human cell lines. *Mol System Biol* 6, 450.

McKenna A, Nordt SP, Ryan J, (2004) Acute nutmeg poisoning. *Eur J Energ Med* 11, 240-241.

Müller, TD, Nogueiras R, Andermannm ML, Andrew ZB, et al., (2015) Ghrelin. *Mol Metabolism* 4, 437-460.

Müller, TD, Blühler M, Tschöp MH, DiMarchi RD, (2022) Anti-obesity drug discovery: advances and challenges. *Nature Rev Drug Discovery* 21, 201-223.

Nguyen PH, Le TVT, Kang HW, Chae J, et al., (2010) AMP-activated protein kinase (AMPK) activators from *Myristica fragrans* (nutmeg) and their anti-obesity effect. *Bioorg Med Chem Lett* 20, 4128-4131.

Park J, Nurkolis F, Won H, Yang J, et al., (2023) Could natural products help in the control of obesity? Current insights and future perspectives. *Molecules* 28, 6604.

Perks KL, Ferreira N, Ermer JA, Rudler DL, et al., (2020) Reduced mitochondrial translation prevents diet-induced metabolic dysfunction but not inflammation. *Aging* 12, 19677-19700.

Perumal NL, Do SK, Choi JS, Lee JH et al., (2024) Anti-adipogenic effect and underlying mechanism of lignan-enriched nutmeg extract on 3T3-L1 preadipocytes. *Biomed Rep* 20, 4.

Powell-Wiley TM, Poirier P, Burke LE, Despres JP, et al., (2021) Obesity and cardiovascular disease: A scientific statement from the American Heart Association. *Circulation* 143, e984-e1010.

Qiao J, Wu Y, Ren Y. (2021) The impact of a high-fat diet on bones: potential mechanisms. *Food Funct* 12, 963-975.

Rohm TV, Meier DT, Olefsky JM, Donath MY, (2022) Inflammation in obesity, diabetes, and related

disorders. *Immunity* 55, 31-55.

Saponaro C, Gaggini M, Carli F, Gastaldelli A, (2015) The subtle balance between lipolysis and lipogenesis: A critical point in metabolic homeostasis. *Nutrients* 7, 9453-9474.

Sayed UFSM, Moshawih S, Goh HP, Kifli N, et al., (2023) Natural products as novel anti-obesity agents: insights into mechanisms of action and potential for therapeutic management. *Front Pharmacol* 14, 2023.

Schwartzm MW, Seeley RJ, Zeltser LM, Drewnowski A, et al., (2017) Obesity pathogenesis : An endocrine society scientific statement, *Endoc Rev* 38, 267-296.

Scott CL, Zheng F, De Baetselier P, Martens L, et al., (2016) Bone marrow-derived monocytes give rise to self-renewing and fully differentiated Kupffer cells. *Nat Commun.* 7, 10321.

Shevchenko A, Tomas H, Havli J, Olsen JV, et al., (2006) In-gel digestion for mass spectrometric characterization of proteins and proteomes. *Nature Protocols* 1, 2856-2860.

Smith AD, Fan A, Qin B, Desai N, et al., (2021) IL-25 Treatment Improves Metabolic Syndrome in High-Fat Diet and Genetic Models of Obesity. *Diab Metab Syndr Ob: Targets Ther* 14, 4875-4887.

Sodhi M, S Rezaelanzadeh R, Kezouh A, Etminan M, (2023) Risk of gastrointestinal adverse events associated with glucagon-like peptide-1 receptor agonists for weight loss. *JAMA* 330, 1795-1797.

Stocks B, Gonzalez-Franquesa A, Borg ML, Björnholm M, et al., (2022) Integrated liver and plasma proteomics in obese mice reveals complex metabolic regulation. *Mol Cell Proteom* 21, 100207.

Sundekilde UK, Yde CC, Honore AH, Rae JMC, et al., (2020) An integrated multi-omics analysis defines key pathway alterations in a diet-induced obesity mouse model. *Metabolites* 10, 80.

Ton SH, Chandramouli C, BAK K, (2013) Glycyrrhizic acid: Biological effects on glucose and lipid metabolism. *In* Natural Products, pp 3803-3826, Springer

Trak-Smayra V, Paradis V, Massart J, Nasser S, et al., (2011) Pathology of the liver in obese and diabetic ob/ob and db/db mice fed a standard or high-calorie diet. *Int J Exp Pathol* 92, 413-421.

Tran S, Baba I, Poupel L, Dussaud S, et al., (2020) Impaired Kupffer cell self-renewal alters the liver response to lipid overload during non-alcoholic steatohepatitis. *Immunity* 53, 627-640.

Tyanova S, Temu T, Sinitcyn P, Carlson A, et al., (2016) The Perseus computational platform for comprehensive analysis of (prote)omics data. *Nature Methods* 13, 731.

Wang D, Eraslan B, Wieland T, Hallström et al., (2019) A deep proteome and transcriptome abundance atlas of 29 healthy human tissues. *Mol Syst Biol* 15, e8503.

Wei F, Gu Y, He L, Kapoor A, et al., (2023) HSD17B6 delays type 2 diabetes development via inhibiting SREBP activation. *Metabolism* 145, 155631

Wohl GR, Loehrke L, Watkins BA, Zernicke RF, (1998) Effects of high-fat diet on mature bone mineral content, structure, and mechanical properties. *Calcif Tissue Int* 63, 74-79.

Wong SK, Chin KY, Suhaimi FHJ, Fairus A, et al., (2016) Animal models of metabolic syndrome: a review. *Nutrition and Metabolism* 13, 65.

Yang XD, Ge XC, Jiang SY, Yang YY, (2022) Potential lipolytic regulators derived from natural products as effective approaches to treat obesity. *Front Endocrinol* 13, 1-14.

Yanovski SZ, Yanovski JA, (2014) Long-term drug treatment for obesity: A systemic and clinical review. *JAMA* 311, 74-86.

Zhao W, Guo M, Feng J, Gu Z, et al., (2022) *Myristica fragrans* extract regulates gut microbes and metabolites to attenuate hepatic inflammation and lipid metabolism disorders via the AhR-FAS and NF-κB signaling pathways in mice with non-alcoholic fatty liver disease. *Nutrients* 14, 1699.

Zhang Y, Proenca R, Maffel M, Barone M, et al., (1994) Positional cloning of the mouse obese gene and its human homologue. *Nature* 372, 425-432.

국문 초록

고지방식 마우스에서 리그난 강화 육두구 추출물의 항비만효과

양 재 호

대전대학교 대학원 한의학과 한방내과학III전공
(지도교수 유 화 승)

비만은 2형 당뇨병, 심혈관 질환, 고지혈증 및 심각한 경우에는 암과 같은 이차적인 상태로 이어질 수 있는 대사 이상이다. 비만약은 개발되어 있지만, 약물 의존성과 부작용 같은 문제가 여전히 남아있다. 따라서 천연물 유래 추출물이 비만치료제의 대안으로 고려되고 있다. 오랫동안 전통 의학으로 사용된 육두구는 독성 물질인 미리스티신 등이 함유되어 있지만 우수한 약리작용을 나타내는 리그난 화합물을 상당량 함유하고 있다. 본 연구에서는 리그난 (특히, nectandrin B)이 농축된 육두구 추출물 (LNX)의 항비만 효과를 비만 마우스 모델을 사용하여 조사하였다. 고지방식으로 자연적 비만을 유도하고 동시에 LNX를 고지방식과 함께 섭식하여 비만 마우스의 생리적 및 분자 수준에서 항비만 유전자/단백질을 탐색하였다. HFD로 6개월 동안 비만 과정을 관찰하였다. 정상식이 (ND) 대비 고지방식 (HFD)에서는 체중증가가 유의적으로

증가하였으며 특히, 체지방%가 크게 증가하였는데 LNX를 섭취한 그룹은 지방축적이 크게 감소하였다. HFD로 인해 혈당 및 총 콜레스테롤 수치가 증가하였지만 LNX로 큰 폭으로 감소하였으며 중성지방 및 LDL 콜레스테롤 수치도 감소하였다. DEXA를 통한 체지방 분석에서는 LNX에 의해 체지방량이 크게 감소하였으며 지방 세포의 크기와 면적이 LNX에 의해 크게 감소하였다. 정상식이과 고지방식 그리고 LNX를 함께 섞은 고지방식 마우스의 간을 적출하여 mRNA와 단백질의 발현 양상을 비교하였다. 전사체 발현 양상은 LNX에 의해 6종이 증가하였고 6종은 감소하였다. 이중 단백질 발현으로 확인된 것은 3종이었다. 단백질체 비교 분석에서는 LNX에 의해 7종의 단백질이 증가하였고 19종은 감소하였다. 단백체와 전사체의 발현 상관관계는 거의 없는 것으로 확인되었다. 종합적으로 LNX에 의해 mRNA와 단백질의 발현체가 공통으로 변화된 것은 6종 (Thrsp, Hsd17b6, Cyp51, Clec4f, S100a9, Krt23)으로 나타났다. 이들 LNX 표적 발현체들은 지질대사와 콜레스테롤 합성, 면역반응과 상피세포 분화에 관련되어 있다. 향후, LNX의 표적 유전자/단백질의 분자수준에서 규명을 통해 새로운 비만치료제 개발의 새로운 방법과 작용기전을 규명할 수 있을 것으로 추정한다.

주요 용어: 항비만, 리그난 농축 육두구 추출물, 전사체, 단백체 분석

Abstract

Anti-obesity Effects of Lignan-enriched Nutmeg Extracts in High-fat Diet Mouse

Jae Ho Yang

Major in Korean Internal Medicine III

Department of Korean Medicine

Graduate School, Daejeon University

(Supervisor Professor Hwa-Seung Yoo)

Obesity is a metabolic disorder that can lead to secondary conditions such as type 2 diabetes, cardiovascular diseases, hyperlipidemia, and, in severe cases, even cancer. Although pharmacotherapy for obesity has been developed, challenges such as drug dependence and side effects persist. Therefore, natural product-derived extracts are being considered as alternative anti-obesity drugs. Nutmeg, traditionally used in traditional medicine, contains toxic substances

such as myristicin but is rich in lignan compounds with excellent pharmacological effects. This study aimed at investigating the anti-obesity effects of lignan-enriched nutmeg extract (LNX), particularly nectandrin B, in a mouse model of obesity. Obesity was induced naturally by a high-fat diet (HFD), and at the same time, LNX was administered along with the high-fat diet to explore the physiological and molecular levels of anti-obesity genes/proteins in obese mice. The obesity process was observed for 6 months under an HFD. In comparison to a normal diet (ND), the high-fat diet (HFD) significantly increased body weight, especially a considerable increase in body fat percentage. However, the group that consumed LNX with HFD showed a significant reduction in fat accumulation. Additionally, blood glucose and total cholesterol levels increased with HFD but decreased significantly with LNX, including a reduction in triglyceride and LDL cholesterol levels. DEXA analysis of body fat showed a significant reduction in body fat mass with LNX, and the size and area of fat cells were greatly reduced. To compare the expression patterns of mRNA and proteins, the liver was extracted from mice fed a normal diet, a high-fat diet, and a high-fat diet mixed with LNX. Transcriptome analysis showed an increase in six genes and a decrease in seven genes due to LNX. Three of these changes were confirmed at the protein level. Proteome comparison analysis revealed an increase in seven proteins and a decrease in 19 proteins due to LNX. There was almost no correlation between the expression of proteins and transcripts. Overall, six common genes/proteins were found to be altered by LNX at the molecular level (Thrsp, Hsd17b6, Cyp51, Clec4f, S100a9, Krt23). These targeted expression profiles of LNX are related to lipid metabolism, cholesterol synthesis, immune response, and epithelial cell differentiation. In the future, elucidating the molecular level of these targeted genes/proteins of LNX is expected to contribute to the development of new anti-obesity agents and the understanding of their mechanisms of action.

Keywords: Anti-obesity, lignan-enriched nutmeg extract, transcriptome analysis, proteome analysis